

# IMPROVING THE ACCURACY-ROBUSTNESS TRADE-OFF OF CLASSIFIERS VIA ADAPTIVE SMOOTHING\*

Yatong Bai<sup>1</sup>, Brendon G. Anderson<sup>1</sup>, Aerin Kim<sup>2</sup>, Somayeh Sojoudi<sup>1</sup>

<sup>1</sup>*University of California, Berkeley*

<sup>2</sup>*Scale AI*

{yatong\_bai, bganderson, sojoudi}@berkeley.edu, aerinykim@gmail.com

– *Abstract* –

While prior research has proposed a plethora of methods that enhance the adversarial robustness of neural classifiers, practitioners are still reluctant to adopt these techniques due to their unacceptably severe penalties in clean accuracy. This paper shows that by mixing the output probabilities of a standard classifier and a robust model, where the standard network is optimized for clean accuracy and is not robust in general, this accuracy-robustness trade-off can be significantly alleviated. We show that the robust base classifier’s confidence difference for correct and incorrect examples is the key ingredient of this improvement. In addition to providing intuitive and empirical evidence, we also theoretically certify the robustness of the mixed classifier under realistic assumptions. Furthermore, we adapt an adversarial input detector into a mixing network that adaptively adjusts the mixture of the two base models, further reducing the accuracy penalty of achieving robustness. The proposed flexible method, termed “adaptive smoothing”, can work in conjunction with existing or even future methods that improve clean accuracy, robustness, or adversary detection. Our empirical evaluation considers strong attack methods, including AutoAttack and adaptive attack. On the CIFAR-100 dataset, our method achieves an 85.21% clean accuracy while maintaining a 38.72%  $\ell_\infty$ -AutoAttacked ( $\epsilon = 8/255$ ) accuracy, becoming the second most robust method on the RobustBench CIFAR-100 benchmark as of submission, while improving the clean accuracy by ten percentage points compared with all listed models. The code that implements our method is available at <https://github.com/Bai-YT/AdaptiveSmoothing>.

## 1. Introduction

Neural networks are vulnerable to adversarial attacks in various applications, including computer vision [34, 57], natural language processing [33], and control systems [41]. Due to the widespread application of neural classifiers, ensuring their reliability in practice is paramount.

To mitigate this susceptibility, researchers have explored “adversarial training” [15, 16, 34, 47, 80], an empirical technique that trains neural networks on adversarial examples to build robust models. Since its initial introduction, multiple improved variants of adversarial training have been devised to enhance the performance of robust classifiers. On the theoretical side, researchers have also considered ensuring the certified robustness of neural classifiers, which mathematically guarantees a

---

\*This work is an extension of [14], and was supported by grants from ONR, NSF, and C3 AI.

model’s robustness to adversarial attacks [7, 9, 54] within a radius. “Randomized smoothing” (RS) is one such method that seeks to achieve certified robustness of an existing model at inference time [25, 50], with improved variants incorporating dimension reduction methods [63] and denoising diffusion components [19], thereby certifying much larger radii. Recent work [8] has demonstrated that a locally biased smoothing approach can improve over traditional data-blind randomized smoothing. However, this method is limited to binary classification problems and suffers from the performance bottleneck of its underlying one-nearest-neighbor classifier.

Despite the emergence of these proposed remedies to the adversarial robustness issue, many practitioners are reluctant to adopt them. As a result, existing publicly available services are still vulnerable [18, 42], presenting severe safety risks. One important reason for this reluctance is the potential for significantly reduced model performance on clean data. Specifically, some previous works have suggested a fundamental trade-off between accuracy and robustness [73, 79]. Since the sacrifice in unattacked performance is understandably unacceptable in real-world scenarios, developing robust classifiers with minimal clean accuracy degradation is crucial.

Fortunately, recent research has argued that it should be possible to simultaneously achieve robustness and accuracy on benchmark datasets [77]. To this end, variants of adversarial training that improve the accuracy-robustness trade-off have been proposed, including TRADES [79], Interpolated Adversarial Training [48], and many others [13, 17, 64, 72, 75, 78]. However, despite these improvements, degraded clean accuracy is often an inevitable price of achieving robustness. Moreover, standard non-robust models often achieve enormous performance gains by pre-training on larger datasets. In contrast, the effect of pre-training on robust classifiers is less understood and may be less prominent [23, 31]. As a result, the performance gap between these existing works and the possibility guaranteed in [77] is still huge.

This work builds upon locally biased smoothing [8] and makes a theoretically disciplined step towards performing robust classification without sacrificing clean accuracy, significantly closing this performance gap and thereby providing practitioners additional incentives for deploying robust models. We summarize our contributions below.

- In Section 3, under the observation that the performance of the  $K$ -nearest-neighbor ( $K$ -NN) classifier, a crucial component of locally biased smoothing, becomes a bottleneck of the overall performance, we replace the  $K$ -NN classifier with a robust neural network that can be obtained via various existing methods, and modify the smoothing formulation accordingly. The resulting formulation (4) is a convex combination of the outputs of a standard neural network and a robust neural network. When the robust neural network has a certified Lipschitz constant or is based on randomized smoothing, the combined classifier also has a closed-form certified robust radius. This section, along with the corresponding experiment results in Sec. 5.2 and Appendix A, are also presented in our conference submission [14].
- In Section 4, we propose an adaptive smoothing procedure that adaptively adjusts the mixture of a standard model and a robust model by adopting a type of adversary detector as a “mixing network”. The mixing network adjusts the convex combination of the outputs (probabilities) from two networks, further improving the accuracy-robustness trade-off. We then empirically verify the robustness of the proposed method using gray-box and white-box projected gradient descent (PGD) attack, AutoAttack, and adaptive attack, demonstrating that the mixing network is robust against the types of adversaries it is trained with. When

the mixing network is trained with examples generated by a carefully constructed adaptive AutoAttack, the composite model sacrifices little robustness while significantly enhancing the clean accuracy. The results in this section and the corresponding experiment results are entirely new contributions relative to our conference submission [14], and are crucial for achieving the much improved accuracy-robustness trade-off compared with existing works.

Note that adaptive smoothing is agnostic to the method of obtaining standard and robust base models. Thus, adaptive smoothing can take advantage of pre-training on large datasets via the standard base classifier and benefit from ongoing advancements in robust training methods via the robust base classifier.

## 2. Background and related works

### 2.1. Notations

The symbol  $\|\cdot\|_p$  denotes the  $\ell_p$  norm of a vector, while  $\|\cdot\|_{p^*}$  denotes its dual norm. The matrix  $I_d$  denotes the identity matrix in  $\mathbb{R}^{d \times d}$ . For a scalar  $a$ ,  $\text{sgn}(a) \in \{-1, 0, 1\}$  denotes its sign. For a natural number  $c$ ,  $[c] = \{1, 2, \dots, c\}$ . For an event  $A$ , the indicator function  $\mathbb{I}(A)$  evaluates to 1 if  $A$  takes place and 0 otherwise. The notation  $\mathbb{P}_{X \sim \mathcal{S}}[A(X)]$  denotes the probability for an event  $A(X)$  to occur, where  $X$  is a random variable drawn from the distribution  $\mathcal{S}$ .

Consider a model  $g : \mathbb{R}^d \rightarrow \mathbb{R}^c$ , whose components are  $g_i : \mathbb{R}^d \rightarrow \mathbb{R}$ ,  $i \in [c]$ , where  $d$  is the dimension of the input and  $c$  is the number of classes. A classifier  $f : \mathbb{R}^d \rightarrow [c]$  can be obtained via  $f(x) \in \arg \max_{i \in [c]} g_i(x)$ . In this paper, we assume that  $g(\cdot)$  does not have the desired level of robustness, and refer to it as a “standard classifier” (as opposed to a “robust classifier” which we denote as  $h(\cdot)$ ). We use  $\mathcal{D}$  to denote the set of all validation input-label pairs  $(x_i, y_i)$ .

We consider  $\ell_p$ -norm-bounded attacks on differentiable neural networks. A classifier  $f(\cdot)$  is considered robust against adversarial perturbations at an input data  $x \in \mathbb{R}^d$  if it assigns the same label to all perturbed inputs  $x + \delta$  such that  $\|\delta\|_p \leq \epsilon$ , where  $\epsilon \geq 0$  is the attack radius.

### 2.2. Related adversarial attacks and defenses

The fast gradient sign method (FGSM) and PGD attacks based on the first-order maximization of the cross-entropy loss have traditionally been considered classic and straightforward attacks [34, 55]. However, these attacks have been shown to be insufficient as defenses designed against them are often easily circumvented [11, 12, 21, 62]. To this end, various attack methods based on alternative loss functions, Expectation Over Transformation, and black-box perturbations have been proposed. Such efforts include MultiTargeted attack loss [37], AutoAttack [29], adaptive attack [71], minimal distortion attack [28], and many others, even considering attacking test-time defenses [27]. The diversity of attack methods has led to the creation of benchmarks such as RobustBench [26] and ARES-Bench [51] to unify the evaluation of robust models.

On the defense side, while adversarial training [55] and TRADES [79] have seen enormous success, such methods are often limited by a significantly larger amount of required training data [68]. Initiatives that construct more effective training data via data augmentation [35, 36, 65] and generative models [69, 76] have successfully produced more accurate and robust models. Improved versions of adversarial training [43, 59, 70, 74] have also been proposed.

Previous research has developed models that improve robustness by dynamically changing at test time. Specifically, “Input-Adaptive Inference” improves the accuracy-robustness trade-off by appending side branches to a single network, allowing for early-exit predictions [40]. Other initiatives that aim to enhance the accuracy-robustness trade-off include using the SCORE attack during training [60] and applying adversarial training for regularization [81].

Moreover, ensemble-based defenses, such as random ensemble [52], diverse ensemble [1, 3, 61], and Jacobian ensemble [24], have been proposed. In comparison, this work is distinct in that our mixing scheme uses two separate classifiers, incorporating one non-robust component while still ensuring the adversarial robustness of the overall design. By doing so, we take advantage of the high performance of modern pre-trained models, significantly alleviating the accuracy-robustness trade-off and achieving much higher overall performances. Additionally, unlike some previous ensemble initiatives, our formulation is deterministic and straightforward, making it easier to evaluate its robustness properly.

### 2.3. Locally biased smoothing

Randomized smoothing, popularized by [25], achieves robustness at test time by replacing  $f(x)$  with a smoothed classifier, given by

$$\tilde{f}(x) \in \arg \max_{i \in [c]} \mathbb{P}_{\delta \sim \mathcal{S}}[f(x + \delta) = i],$$

where  $\mathcal{S}$  is a smoothing distribution. A common choice for  $\mathcal{S}$  is a Gaussian distribution.

The authors of [8] have recently argued that data-invariant randomized smoothing does not always achieve robustness. They have shown that in the binary classification setting, randomized smoothing with an unbiased distribution is suboptimal, and an optimal smoothing procedure shifts the input point in the direction of its true class. Since the true class is generally unavailable, a “direction oracle” is used as a surrogate. This “locally biased smoothing” method is no longer randomized and outperforms traditional data-blind randomized smoothing. The locally biased smoothed classifier  $h^\gamma(\cdot)$  is obtained via the deterministic calculation

$$h^\gamma(x) = g(x) + \gamma h(x) \|\nabla g(x)\|_{p^*},$$

where  $h(x) \in \{-1, 1\}$  is the direction oracle and  $\gamma \geq 0$  is a trade-off parameter. The direction oracle should come from an inherently robust classifier (which is often less accurate). In [8], this direction oracle is chosen to be a one-nearest-neighbor classifier.

### 2.4. Adversarial input detectors

It has been shown that adversarial inputs can be detected via various methods. For example, [56] proposes to append an additional detection branch to an existing neural network, and uses adaptive adversarial data to train the detector in a supervised fashion. However, [20] has shown that it is possible to bypass this detection method. They constructed adversarial examples via the C&W attacks [21] and simultaneously targeted the classification branch and the detection branch by treating the two branches as an “augmented classifier”. According to [20], the detector is effective against the types of attack that it is trained with, but not necessarily the attack types that are absent in the training data. It is thus reasonable to expect the detector to be able to detect a wide

range of attacks if it is trained using sufficiently diverse types of attacks (including those targeting the detector itself). While exhaustively covering the entire adversarial input space is intractable, and it is unclear to what degree one needs to diversify the attack types in practice, our experiments show that our modified architecture based on [56] can recognize the state-of-the-art AutoAttack adversaries with a high success rate.

The literature has also considered alternative detection methods that mitigate the above challenges faced by detectors trained in a supervised fashion [22]. Such initiatives include unsupervised detectors [4, 5] and re-attacking [2]. Since universally effective detectors have not yet been discovered, this paper focuses on transferring the properties of the existing detector toward better overall robustness. Future advancements in the field of adversary detection can further enhance the performance of our method.

### 3. Using a robust neural network as the smoothing oracle

Since locally biased smoothing was designed for binary classification problems, we first extend it to the multi-class setting. To achieve this, we treat the output  $h_i^\gamma(x)$  of each class independently, giving rise to:

$$h_{\text{smo1},i}^\gamma(x) := g_i(x) + \gamma h_i(x) \|\nabla g_i(x)\|_{p^*}, \quad i \in [c]. \quad (1)$$

Note that if  $\|\nabla g_i(x)\|_{p^*}$  is large for some  $i$ , then  $h_{\text{smo1},i}^\gamma(x)$  can be large even if both  $g_i(x)$  and  $h_i(x)$  are small, potentially leading to incorrect predictions. To remove the effect of the magnitude difference across the classes, we propose a normalized formulation as follows:

$$h_{\text{smo2},i}^\gamma(x) := \frac{g_i(x) + \gamma h_i(x) \|\nabla g_i(x)\|_{p^*}}{1 + \gamma \|\nabla g_i(x)\|_{p^*}}, \quad i \in [c]. \quad (2)$$

The parameter  $\gamma$  adjusts the trade-off between clean accuracy and robustness. When  $\gamma = 0$ , it holds that  $h_{\text{smo2},i}^\gamma(x) \equiv g_i(x)$  for all  $i$ . When  $\gamma \rightarrow \infty$ , it holds that  $h_{\text{smo2},i}^\gamma(x) \rightarrow h_i(x)$  for all  $x$  and all  $i$ .

With the mixing procedure generalized to the multi-class setting, we now discuss the choice of the smoothing oracle  $h_i(\cdot)$ . While  $K$ -NN classifiers are relatively robust and can be used as the oracle, their representation power is too weak. On the CIFAR-10 image classification task [46],  $K$ -NN only achieves around 35% accuracy on clean test data. In contrast, an adversarially trained ResNet [38] can reach 50% accuracy on attacked test data [55]. This lackluster performance of  $K$ -NN becomes a significant bottleneck in the accuracy-robustness trade-off of the mixed classifier. To this end, we replace the  $K$ -NN model with a robust neural network. The robustness of this network can be achieved via various methods, including adversarial training, TRADES, and traditional randomized smoothing.

Further scrutinizing (2) leads to the question of whether  $\|\nabla g_i(x)\|_{p^*}$  is the best choice for adjusting the mixture of  $g(\cdot)$  and  $h(\cdot)$ . In fact, this gradient magnitude term is a result of the assumption that  $h(x) \in \{-1, 1\}$ , which is the setting considered in [8]. Here, we no longer have this assumption. Instead, we assume both  $g(\cdot)$  and  $h(\cdot)$  to be differentiable. Thus, we further generalize the formulation to

$$h_{\text{smo3},i}^\gamma(x) := \frac{g_i(x) + \gamma R_i(x) h_i(x)}{1 + \gamma R_i(x)}, \quad i \in [c], \quad (3)$$

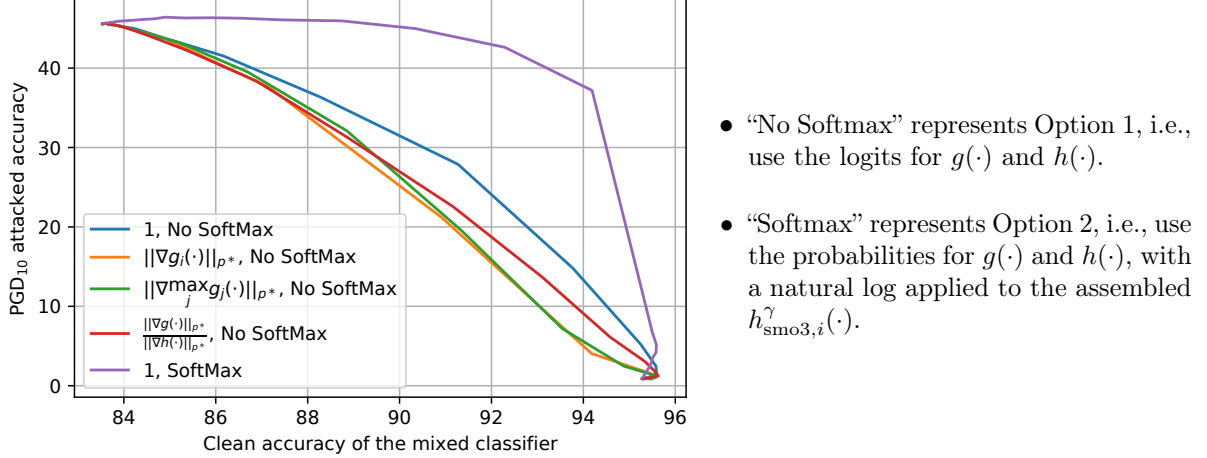


**Figure 1.** Comparing the “attacked accuracy versus clean accuracy” curve for various options for  $R_i(x)$ . Note that with the best formulation, high clean accuracy can be achieved with very little sacrifice on robustness.

where  $R_i(x)$  is an extra scalar term that can potentially depend on both  $\nabla g_i(x)$  and  $\nabla h_i(x)$  to determine the “trustworthiness” of the base classifiers. Here, we empirically compare four options for  $R_i(x)$ , namely, 1,  $\|\nabla g_i(x)\|_{p^*}$ ,  $\|\nabla \max_j g_j(x)\|_{p^*}$ , and  $\frac{\|\nabla g_i(x)\|_{p^*}}{\|\nabla h_i(x)\|_{p^*}}$ .

Another design question is whether  $g(\cdot)$  and  $h(\cdot)$  should be the pre-softmax logits or the post-softmax probabilities. Note that since most attack methods are designed based on logits, the output of the mixed classifier should be logits rather than probabilities to avoid gradient masking, an undesirable phenomenon that makes it hard to evaluate the proposed method properly. Thus, we have the following two options that make the mixed model compatible with existing gradient-based attacks:

1. Use the logits for both  $g(\cdot)$  and  $h(\cdot)$ .
2. Use the probabilities for both  $g(\cdot)$  and  $h(\cdot)$ , and then convert the mixed probabilities back to logits. The required “inverse-softmax” operator is given simply by the natural logarithm, and does not change the prediction.

In Fig. 1, we compare the different choices for  $R_i(x)$  by visualizing the accuracy-robustness trade-off. Based on this “clean accuracy versus PGD<sub>10</sub>-attacked accuracy” plot, where PGD<sub>T</sub> denotes  $T$ -step PGD, we conclude that  $R_i(x) = 1$  gives the best accuracy-robustness trade-off, and  $g(\cdot)$  and  $h(\cdot)$  should be the probabilities.

In later sections, we will offer additional theoretical and empirical justifications for this choice. Specifically, in addition to the set of base classifiers (a pair of standard and adversarially trained ResNet-18s) considered in Fig. 1, we provide examples in Appendix A using alternative model architectures, different methods to train the robust base classifiers, and various attack budgets, all of which lead to the same best choice for  $R_i(x)$ . With these design choices implemented, the formulation (3) can be re-parameterized as

$$h_i^\alpha(x) := \log((1 - \alpha)g_i(x) + \alpha h_i(x)), \quad i \in [c], \quad (4)$$



where  $\alpha = \frac{\gamma}{1+\gamma} \in [0, 1]$ . We take  $h^\alpha(\cdot)$  in (4), which outputs the natural logarithm of a convex combination of the probabilities  $g(\cdot)$  and  $h(\cdot)$ , as our proposed mixed classifier.

### 3.1. Theoretical certified robust radius

In this section, we derive certified robust radii for  $h^\alpha(\cdot)$  introduced in (4), given in terms of the robustness properties of  $h(\cdot)$  and the mixing parameter  $\alpha$ . The results ensure that despite being more sophisticated than a single model,  $h^\alpha(\cdot)$  cannot be easily conquered, even if an adversary attempts to adapt its attack methods to its structure. Such guarantees are of paramount importance for reliable deployment in safety-critical control applications. Since we use probabilities for  $g(\cdot)$  and  $h(\cdot)$ , it holds that  $0 \leq g_i(\cdot) \leq 1$  and  $0 \leq h_i(\cdot) \leq 1$  for all  $i$ . To facilitate the proofs, we introduce the following generalized notion of certified robustness.

**Definition 1.** Consider a model  $h : \mathbb{R}^d \rightarrow \mathbb{R}^c$  and an arbitrary input  $x \in \mathbb{R}^d$ . Further consider  $y = \arg \max_i h_i(x)$ ,  $\mu \in [0, 1]$ , and  $r \geq 0$ . Then,  $h(\cdot)$  is said to be *certifiably robust at  $x$  with margin  $\mu$  and radius  $r$*  if  $h_y(x + \delta) \geq h_i(x + \delta) + \mu$  for all  $i \neq y$  and all  $\delta \in \mathbb{R}^d$  such that  $\|\delta\|_p \leq r$ .

**Lemma 1.** Let  $x \in \mathbb{R}^d$  and  $r \geq 0$ . If it holds that  $\alpha \in [\frac{1}{2}, 1]$  and  $h(\cdot)$  is certifiably robust at  $x$  with margin  $\frac{1-\alpha}{\alpha}$  and radius  $r$ , then the mixed classifier  $h^\alpha(\cdot)$  is robust in the sense that  $\arg \max_i h_i^\alpha(x + \delta) = \arg \max_i h_i(x)$  for all  $\delta \in \mathbb{R}^d$  such that  $\|\delta\|_p \leq r$ .

*Proof.* Suppose that  $h(\cdot)$  is certifiably robust at  $x$  with margin  $\frac{1-\alpha}{\alpha}$  and radius  $r$ . Since  $\alpha \in [\frac{1}{2}, 1]$ , it holds that  $\frac{1-\alpha}{\alpha} \in [0, 1]$ . Let  $y = \arg \max_i h_i(x)$ . Consider an arbitrary  $i \in [c] \setminus \{y\}$  and  $\delta \in \mathbb{R}^d$  such that  $\|\delta\|_p \leq r$ . Since  $g_i(x + \delta) \in [0, 1]$ , it holds that

$$\begin{aligned} \exp(h_y^\alpha(x + \delta)) - \exp(h_i^\alpha(x + \delta)) &= (1 - \alpha)(g_y(x + \delta) - g_i(x + \delta)) + \alpha(h_y(x + \delta) - h_i(x + \delta)) \\ &\geq (1 - \alpha)(0 - 1) + \alpha(h_y(x + \delta) - h_i(x + \delta)) \\ &\geq (\alpha - 1) + \alpha \left( \frac{1-\alpha}{\alpha} \right) = 0. \end{aligned}$$

Thus, it holds that  $h_y^\alpha(x + \delta) \geq h_i^\alpha(x + \delta)$  for all  $i \neq y$ , and thus  $\arg \max_i h_i^\alpha(x + \delta) = y = \arg \max_i h_i(x)$ .  $\square$

Lemma 1 provides further justifications for using probabilities instead of logits in the smoothing operation. Intuitively, it holds that  $(1 - \alpha)g_i(\cdot)$  is bounded between 0 and  $1 - \alpha$ , so as long as  $\alpha$  is relatively large (specifically, at least  $\frac{1}{2}$ ), the detrimental effect of  $g(\cdot)$  when subject to attack can be overcome by  $h(\cdot)$ . On the other hand, if each  $g_i(\cdot)$  is the logit, then it cannot be bounded, and thus it is much harder to overcome its vulnerability.

Since we do not make assumptions on the Lipschitzness or robustness of  $g(\cdot)$ , Lemma 1 is tight. To understand this, we suppose that there exists some  $i \in [c] \setminus \{y\}$  and  $\delta \neq 0$  such that  $\|\delta\|_p \leq r$  that make  $h_y(x + \delta) - h_i(x + \delta) := h_d$  smaller than  $\frac{1-\alpha}{\alpha}$ , indicating that  $-\alpha h_d > \alpha - 1$ . Since the only information about  $g(\cdot)$  is that  $g_i(x + \delta) \in [0, 1]$  and thus the value  $g_y(x + \delta) - g_i(x + \delta)$  can be any number in  $[-1, 1]$ , it is possible that  $(1 - \alpha)(g_y(x + \delta) - g_i(x + \delta))$  is smaller than  $-\alpha h_d$ . In this case, it holds that  $h_y^\alpha(x + \delta) < h_i^\alpha(x + \delta)$ , and thus  $\arg \max_i h_i^\alpha(x + \delta) \neq \arg \max_i h_i(x)$ .

While most certifiably robust models consider the special case where the margin is zero, we will show that models built via common methods are also robust with non-zero margins, and can thus take advantage of Lemma 1. Specifically, we consider two types of popular robust classifiers: Lipschitz continuous models (Theorem 1) and RS models (Theorem 2).

**Definition 2.** A function  $f: \mathbb{R}^d \rightarrow \mathbb{R}$  is called  $\ell_p$ -Lipschitz continuous if there exists  $L \in (0, \infty)$  such that  $|f(x') - f(x)| \leq L\|x' - x\|_p$  for all  $x', x \in \mathbb{R}^d$ . The Lipschitz constant of such  $f$  is defined to be  $\text{Lip}_p(f) := \inf\{L \in (0, \infty) : |f(x') - f(x)| \leq L\|x' - x\|_p \text{ for all } x', x \in \mathbb{R}^d\}$ .

**Assumption 1.** The classifier  $h(\cdot)$  is robust in the sense that, for all  $i \in \{1, 2, \dots, n\}$ ,  $h_i(\cdot)$  is  $\ell_p$ -Lipschitz continuous with Lipschitz constant  $\text{Lip}_p(h_i)$ .

Assumption 1 is not restrictive in practice. For example, Gaussian RS with smoothing variance  $\sigma^2 I_d$  yields robust models with  $\ell_2$ -Lipschitz constant  $\sqrt{\frac{2}{\pi\sigma^2}}$  [67]. Moreover, empirically robust methods such as adversarial training and TRADES often train Lipschitz continuous models, even though there may not be closed-form theoretical guarantees.

**Theorem 1.** Suppose that Assumption 1 holds, and let  $x \in \mathbb{R}^d$  be arbitrary. Let  $y = \arg \max_i h_i(x)$ . Then, if  $\alpha \in [\frac{1}{2}, 1]$ , it holds that  $\arg \max_i h_i^\alpha(x + \delta) = y$  for all  $\delta \in \mathbb{R}^d$  such that

$$\|\delta\|_p \leq r_{\text{Lip},p}^\alpha(x) := \min_{i \neq y} \frac{\alpha(h_y(x) - h_i(x)) + \alpha - 1}{\alpha(\text{Lip}_p(h_y) + \text{Lip}_p(h_i))}.$$

*Proof.* Suppose that  $\alpha \in [\frac{1}{2}, 1]$ , and let  $\delta \in \mathbb{R}^d$  be such that  $\|\delta\|_p \leq r_{\text{Lip},p}^\alpha(x)$ . Furthermore, let  $i \in [c] \setminus \{y\}$ . It holds that

$$\begin{aligned} h_y(x + \delta) - h_i(x + \delta) &= h_y(x) - h_i(x) + h_y(x + \delta) - h_y(x) + h_i(x) - h_i(x + \delta) \\ &\geq h_y(x) - h_i(x) - \text{Lip}_p(h_y)\|\delta\|_p - \text{Lip}_p(h_i)\|\delta\|_p \\ &\geq h_y(x) - h_i(x) - (\text{Lip}_p(h_y) + \text{Lip}_p(h_i)) r_{\text{Lip},p}^\alpha(x) \geq \frac{1-\alpha}{\alpha}. \end{aligned}$$

Therefore,  $h(\cdot)$  is certifiably robust at  $x$  with margin  $\frac{1-\alpha}{\alpha}$  and radius  $r_{\text{Lip},p}^\alpha(x)$ . Hence, by Lemma 1, the claim holds.  $\square$

We remark that the  $\ell_p$  norm that we certify using Theorem 1 may be arbitrary (e.g.,  $\ell_1$ ,  $\ell_2$ , or  $\ell_\infty$ ), so long as the Lipschitz constant of the robust network  $h(\cdot)$  is computed with respect to the same norm.

If  $\alpha \rightarrow 1$ , then  $r_{\text{Lip},p}^\alpha(x) \rightarrow \min_{i \neq y} \frac{h_y(x) - h_i(x)}{\text{Lip}_p(h_y) + \text{Lip}_p(h_i)}$ , which is the standard (global) Lipschitz-based robust radius of  $h(\cdot)$  around  $x$  (see, e.g., [32, 39] for further discussions on Lipschitz-based robustness). On the other hand, if  $\alpha$  is too small in comparison to the relative confidence of  $h(\cdot)$ , namely, if there exists  $i \neq y$  such that  $\alpha \leq \frac{1}{1 + h_y(x) - h_i(x)}$ , then  $r_{\text{Lip},p}^\alpha(x) \leq 0$ , and in this case we cannot provide non-trivial certified robustness for  $h^\alpha(\cdot)$ . This is rooted in the fact that too small of an  $\alpha$  value amounts to an excess weight into the non-robust classifier  $g(\cdot)$ . If  $h(\cdot)$  is 100% confident in its prediction, then  $h_y(x) - h_i(x) = 1$  for all  $i \neq y$ , and therefore this threshold value of  $\alpha$  becomes  $\frac{1}{2}$ , leading to non-trivial certified radii for  $\alpha > \frac{1}{2}$ . However, once we put over  $\frac{1}{2}$  of the weight into  $g(\cdot)$ , a nonzero radius around  $x$  is no longer certifiable. Again, this is intuitively the best one can expect, since no assumptions on the robustness of  $g(\cdot)$  around  $x$  have been made. Theorem 1 clearly generalizes to the even less restrictive scenario of using local Lipschitz constants over a neighborhood  $\mathcal{U}$  of  $x$  as a surrogate for the global Lipschitz constants, so long as the condition  $\delta \in \mathcal{U}$  is also added to the hypotheses.

We now move on to tightening the certified radius in the special case when  $h(\cdot)$  is an RS classifier and our robust radii are defined in terms of the  $\ell_2$  norm.



**Assumption 2.** The classifier  $h(\cdot)$  is a (Gaussian) RS classifier, i.e.,  $h(x) = \mathbb{E}_{\xi \sim \mathcal{N}(0, \sigma^2 I_d)} [\bar{h}(x + \xi)]$  for all  $x \in \mathbb{R}^d$ , where  $\bar{h}: \mathbb{R}^d \rightarrow [0, 1]^c$  is a classifier that is non-robust in general. Furthermore, for all  $i \in [c]$ ,  $\bar{h}_i(\cdot)$  is not 0 almost everywhere or 1 almost everywhere.

**Theorem 2.** Suppose that Assumption 2 holds, and let  $x \in \mathbb{R}^d$  be arbitrary. Let  $y = \arg \max_i h_i(x)$  and  $y' = \arg \max_{i \neq y} h_i(x)$ . Then, if  $\alpha \in [\frac{1}{2}, 1]$ , it holds that  $\arg \max_i h_i^\alpha(x + \delta) = y$  for all  $\delta \in \mathbb{R}^d$  such that

$$\|\delta\|_2 \leq r_\sigma^\alpha(x) := \frac{\sigma}{2} \left( \Phi^{-1}(\alpha h_y(x)) - \Phi^{-1}(\alpha h_{y'}(x) + 1 - \alpha) \right).$$

*Proof.* First, note that since every  $\bar{h}_i(\cdot)$  is not 0 almost everywhere or 1 almost everywhere, it holds that  $h_i(x) \in (0, 1)$  for all  $i$  and all  $x$ . Now, suppose that  $\alpha \in [\frac{1}{2}, 1]$ , and let  $\delta \in \mathbb{R}^d$  be such that  $\|\delta\|_2 \leq r_\sigma^\alpha(x)$ . Let  $\mu_\alpha := \frac{1-\alpha}{\alpha}$  (conversely,  $\alpha = \frac{1}{\mu_\alpha + 1}$ ). We construct a scaled classifier  $\tilde{h}: \mathbb{R}^d \rightarrow \mathbb{R}^c$ , whose  $i^{\text{th}}$  entry is defined as

$$\tilde{h}_i(x) = \begin{cases} \frac{\bar{h}_y(x)}{1 + \mu_\alpha} = \alpha \bar{h}_y(x) & \text{if } i = y, \\ \frac{\bar{h}_i(x) + \mu_\alpha}{1 + \mu_\alpha} = \alpha \bar{h}_i(x) + 1 - \alpha & \text{if } i \neq y. \end{cases}$$

Furthermore, define a scaled RS classifier  $\hat{h}: \mathbb{R}^d \rightarrow \mathbb{R}^c$  by

$$\hat{h}(x) = \mathbb{E}_{\xi \sim \mathcal{N}(0, \sigma^2 I_d)} [\tilde{h}(x + \xi)].$$

Then, since it holds that

$$\begin{aligned} \tilde{h}_y(x) &= \frac{\bar{h}_y(x)}{1 + \mu_\alpha} \in \left(0, \frac{1}{1 + \mu_\alpha}\right) \subseteq (0, 1), \\ \tilde{h}_i(x) &= \frac{\bar{h}_i(x) + \mu_\alpha}{1 + \mu_\alpha} \in \left(\frac{\mu_\alpha}{1 + \mu_\alpha}, 1\right) \subseteq (0, 1), \quad \forall i \neq y, \end{aligned}$$

it must be the case that  $0 < \tilde{h}_i(x) < 1$  for all  $i$  and all  $x$ , and hence, for all  $i$ , the function  $x \mapsto \Phi^{-1}(\hat{h}_i(x))$  is  $\ell_2$ -Lipschitz continuous with Lipschitz constant  $\frac{1}{\sigma}$  (see [49, Lemma 1], or Lemma 2 in [67] and the discussion thereafter). Therefore,

$$\left| \Phi^{-1}(\hat{h}_i(x + \delta)) - \Phi^{-1}(\hat{h}_i(x)) \right| \leq \frac{\|\delta\|_2}{\sigma} \leq \frac{r_\sigma^\alpha(x)}{\sigma} \quad (5)$$

for all  $i$ . Applying (5) for  $i = y$  yields that

$$\Phi^{-1}(\hat{h}_y(x + \delta)) \geq \Phi^{-1}(\hat{h}_y(x)) - \frac{r_\sigma^\alpha(x)}{\sigma}, \quad (6)$$

and, since  $\Phi^{-1}$  is monotonically increasing and  $\hat{h}_i(x) \leq \hat{h}_{y'}(x)$  for all  $i \neq y$ , applying (5) to  $i \neq y$  gives that

$$\Phi^{-1}(\hat{h}_i(x + \delta)) \leq \Phi^{-1}(\hat{h}_i(x)) + \frac{r_\sigma^\alpha(x)}{\sigma} \leq \Phi^{-1}(\hat{h}_{y'}(x)) + \frac{r_\sigma^\alpha(x)}{\sigma}. \quad (7)$$

Subtracting (7) from (6) gives that

$$\Phi^{-1}(\hat{h}_y(x + \delta)) - \Phi^{-1}(\hat{h}_i(x + \delta)) \geq \Phi^{-1}(\hat{h}_y(x)) - \Phi^{-1}(\hat{h}_{y'}(x)) - \frac{2r_\sigma^\alpha(x)}{\sigma}$$

for all  $i \neq y$ . By the definitions of  $\mu_\alpha$ ,  $r_\sigma^\alpha(x)$ , and  $\hat{h}(x)$ , the right-hand side of this inequality equals zero, and hence, since  $\Phi$  is monotonically increasing, we find that  $\hat{h}_y(x + \delta) \geq \hat{h}_i(x + \delta)$  for all  $i \neq y$ . Therefore,

$$\begin{aligned} \frac{h_y(x + \delta)}{1 + \mu_\alpha} &= \mathbb{E}_{\xi \sim \mathcal{N}(0, \sigma^2 I_d)} \left[ \frac{\bar{h}_y(x + \delta + \xi)}{1 + \mu_\alpha} \right] = \hat{h}_y(x + \delta) \\ &\geq \hat{h}_i(x + \delta) = \mathbb{E}_{\xi \sim \mathcal{N}(0, \sigma^2 I_d)} \left[ \frac{\bar{h}_i(x + \delta + \xi) + \mu_\alpha}{1 + \mu_\alpha} \right] = \frac{h_i(x + \delta) + \mu_\alpha}{1 + \mu_\alpha}. \end{aligned}$$

Hence,  $h_y(x + \delta) \geq h_i(x + \delta) + \mu_\alpha$  for all  $i \neq y$ , so  $h(\cdot)$  is certifiably robust at  $x$  with margin  $\mu_\alpha = \frac{1-\alpha}{\alpha}$  and radius  $r_\sigma^\alpha(x)$ . Therefore, by Lemma 1, it holds that  $\arg \max_i h_i^\alpha(x + \delta) = y$  for all  $\delta \in \mathbb{R}^d$  such that  $\|\delta\|_2 \leq r_\sigma^\alpha(x)$ , which concludes the proof.  $\square$

To summarize our certified radii, Theorem 1 applies to very general Lipschitz continuous robust base classifiers  $h(\cdot)$  and arbitrary  $\ell_p$  norms, whereas Theorem 2, applying to the  $\ell_2$  norm and RS base classifiers, strengthens the certified radius by exploiting the stronger Lipschitzness of  $x \mapsto \Phi^{-1}(\hat{h}_i(x))$  arising from the special structure and smoothness granted by Gaussian convolution operations. Theorems 1 and 2 guarantee that our proposed robustification cannot be easily circumvented by adaptive attacks.

## 4. Adaptive smoothing strength with the mixing network

So far,  $\alpha$  has been treated as a fixed hyperparameter. A more intelligent approach is to allow  $\alpha$  to be different for each  $x$  by replacing the constant  $\alpha$  with a function  $\alpha(x)$ . Here, we take  $\alpha(x)$  to be deterministic, as stochastic defenses can be much harder to evaluate.

One motivation for adopting the adaptive trade-off parameter  $\alpha(x)$  is that the optimal  $\alpha^*$  can vary when  $x$  changes. For example, when  $x$  is clean and unperturbed, the standard model  $g(\cdot)$  outperforms the robust model  $h(\cdot)$ . If  $x$  is an attacked input targeting  $g(\cdot)$ , then the robust model  $h(\cdot)$  should be used. However, as shown in Figure 2, if the target of the attack is  $h(\cdot)$ , then even though  $h(\cdot)$  is robust, a better choice is to feed  $x$  into  $g(\cdot)$ . This is because the loss landscapes of  $g(\cdot)$  and  $h(\cdot)$  differ enough that an adversarial perturbation targeting  $h(\cdot)$  is benign to  $g(\cdot)$ .

When the PGD adversary targets a mixed classifier  $h^{\alpha_t}(\cdot)$ , as  $\alpha_t$  varies, the optimal strategy also changes. We provide a visualization in Figure 2 based on the CIFAR-10 dataset. Specifically, we put together a composite model  $h^{\alpha_t}(\cdot)$  using a ResNet-18 standard classifier  $g(\cdot)$  and a ResNet-18 robust classifier  $h(\cdot)$  via (4).<sup>1</sup> Then, we attack  $h^{\alpha_t}(\cdot)$  with different values of  $\alpha_t$  via PGD<sub>20</sub>, save the adversarial instances, and report the accuracy of  $g(\cdot)$  and  $h(\cdot)$  evaluated on these instances. When  $\alpha_t \leq \text{Sigmoid}(5.72) = 0.9967$ , the robust model  $h(\cdot)$  performs better. When  $\alpha_t > 0.9967$ , the standard model  $g(\cdot)$  is more suitable.

Throughout the remainder of this section, we overload the notation  $h^\alpha(\cdot)$  even though  $\alpha(\cdot)$  may be a function of the input, i.e., we define  $h^\alpha(x) = h^{\alpha(x)}(x)$ .

<sup>1</sup>These ResNet-18 classifiers are obtained from [58].

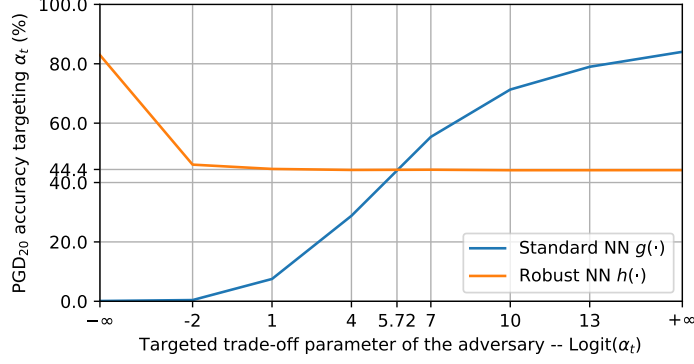


**Figure 2.** Attacked accuracy of the standard classifier  $g(\cdot)$  and the robust classifier  $h(\cdot)$  when the adversary targets different values of  $\alpha_t$ . For better readability, we use  $\text{Logit}(\alpha_t)$  as the horizontal axis labels, where  $\text{Logit}(\cdot)$  denotes the inverse function of Sigmoid.

#### 4.1. The existence of $\alpha(x)$ that achieves the trade-off

The following theorem shows that, under some technical conditions, there exists a function  $\alpha(\cdot)$  that makes the combined classifier correct whenever either  $g(\cdot)$  and  $h(\cdot)$  makes the correct prediction, which further implies that the combined classifier matches the clean accuracy of  $g(\cdot)$  and the attacked accuracy of  $h(\cdot)$ .

**Theorem 3.** Let  $\epsilon > 0$ ,  $(x_1, y_1), (x_2, y_2) \sim \mathcal{D}$ , and  $y_1 \neq y_2$  (i.e., each input corresponds to a unique true label). Assume that  $h_i(\cdot)$ ,  $\|\nabla h_i(\cdot)\|_{p^*}$ , and  $\|\nabla g_i(\cdot)\|_{p^*}$  are all bounded and that there does not exist  $z \in \mathbb{R}^d$  such that  $\|z - x_1\|_p \leq \epsilon$  and  $\|z - x_2\|_p \leq \epsilon$ . Then, there exists a function  $\alpha(\cdot)$  such that the assembled classifier  $h^\alpha(\cdot)$  satisfies

$$\mathbb{P}_{\substack{(x,y) \sim \mathcal{D} \\ \delta \sim \mathcal{F}}} \left[ \arg \max_{i \in [c]} h_i^\alpha(x + \delta) = y \right] \geq \max \left\{ \frac{\mathbb{P}_{(x,y) \sim \mathcal{D}, \delta \sim \mathcal{F}} \left[ \arg \max_{i \in [c]} g_i(x + \delta) = y \right]}{\mathbb{P}_{(x,y) \sim \mathcal{D}, \delta \sim \mathcal{F}} \left[ \arg \max_{i \in [c]} h_i(x + \delta) = y \right]} \right\},$$

where  $\mathcal{F}$  is an arbitrary distribution that satisfies  $\mathbb{P}_{\delta \sim \mathcal{F}} [\|\delta\|_p > \epsilon] = 0$ .

*Proof.* Since it is assumed that the perturbation balls of the data are non-overlapping, the true label  $y$  corresponding to each perturbed data  $x + \delta$  with the property  $\|\delta\|_p \leq \epsilon$  is unique. Therefore, the indicator function

$$\alpha(x + \delta) = \begin{cases} 0 & \text{if } \arg \max_{i \in [c]} g_i(x + \delta) = y, \\ 1 & \text{otherwise,} \end{cases}$$

satisfies that

$$\begin{aligned} \alpha(x + \delta) &= 0 & \text{if } & \arg \max_{i \in [c]} g_i(x + \delta) = y, \\ \alpha(x + \delta) &= 1 & \text{if } & \arg \max_{i \in [c]} g_i(x + \delta) \neq y \text{ and } \arg \max_{i \in [c]} h_i(x + \delta) = y. \end{aligned}$$

Therefore, it holds that

$$\begin{aligned} h_i^\alpha(x + \delta) &= g_i(x + \delta) & \text{if} & \quad \arg \max_{i \in [c]} g_i(x + \delta) = y, \\ h_i^\alpha(x + \delta) &= h_i(x + \delta) & \text{if} & \quad \arg \max_{i \in [c]} g_i(x + \delta) \neq y \text{ and } \arg \max_{i \in [c]} h_i(x + \delta) = y, \end{aligned}$$

implying that

$$\arg \max_{i \in [c]} h_i^\alpha(x + \delta) = y \quad \text{if} \quad (\arg \max_{i \in [c]} g_i(x + \delta) = y \text{ or } \arg \max_{i \in [c]} h_i(x + \delta) = y),$$

which leads to the desired statement.  $\square$

Note that the distribution  $\mathcal{F}$  is arbitrary, implying that the test data can be clean data, any type of adversarial data, or some combination of both. As a special case, when the distribution  $\mathcal{F}$  is a Dirac measure centered at the origin, Theorem 3 implies that the clean accuracy of  $h^\alpha(\cdot)$  is as good as the standard classifier  $g(\cdot)$ . Conversely, when  $\mathcal{F}$  is a Dirac measure centered at the worst-case perturbation, the adversarial accuracy of  $h^\alpha(\cdot)$  is not worse than the robust model  $h(\cdot)$ , implying that if  $h(\cdot)$  is inherently robust, then  $h^\alpha(\cdot)$  inherits the robustness. One can then conclude that there exists a  $h^\alpha(\cdot)$  that matches the clean accuracy of  $g(\cdot)$  and the robustness of  $h(\cdot)$ .

While finding a function  $\alpha(\cdot)$  that perfectly achieves this trade-off is hard, we will use experiments to show that an  $\alpha(\cdot)$  represented by a neural network can retain most of the robustness  $h(\cdot)$  while vastly boosting the clean accuracy. In particular, while we use the case of  $\alpha(\cdot)$  being an indicator function to demonstrate the possibility of achieving the trade-off, letting  $\alpha$  take an appropriate value between 0 and 1 also improves the trade-off, as shown in Fig. 1. Therefore, the task for the neural approximator is easier than representing the indicator function. Furthermore, if certified robustness is desired, one can enforce a lower bound on  $\alpha(\cdot)$  and take advantage of Theorem 1, while still enjoying the mitigated trade-off.

## 4.2. Attacking the adaptive classifier

When the combined model  $h^\alpha(\cdot)$  is under adversarial attack, the function  $\alpha(\cdot)$  provides an additional gradient flow path. Intuitively, the attack should be able to force  $\alpha$  to be small through this additional gradient path, tricking the mixing network to favor the non-robust  $g(\cdot)$ . Following the guidelines for constructing adaptive attacks [71], in the experiments, we consider the following types of attacks:

- A Gray-box PGD<sub>20</sub>:** In this setting, the adversary has access to the gradients of both  $g(\cdot)$  and  $h(\cdot)$  when performing first-order optimization, but is not given the gradient of the mixing network  $\alpha(\cdot)$ . We consider untargeted PGD attack with a fixed initialization.
- B White-box PGD<sub>20</sub>:** Since the mixed classifier is end-to-end differentiable, following [71], we allow the adversary to access the end-to-end gradient, including the gradient of the mixing network.
- C White-box AutoAttack:** “AutoAttack” is a stronger attack formed by an ensemble of four automated attack algorithms [29]. The method considers APGD attacks generated via the untargeted cross-entropy loss and the targeted DLR loss, in addition to the targeted FAB

attack and the black-box Square attack [10]. Again, the end-to-end gradient of the mixed classifier is available to the adversary. AutoAttack requires much more computation budget than PGD<sub>20</sub>.

**D Adaptive white-box AutoAttack:** Since the mixing network is a crucial component of the defense, we adapt AutoAttack to target the mixing network by adding an APGD loss component that aims to decrease  $\alpha$ . We use this additional attack type for evaluation purposes.

We will show that the adaptively smoothed model is robust against the attack that it is trained against. When trained using APGD<sub>75</sub> attack with untargeted and targeted loss functions, our model becomes robust against AutoAttack. Furthermore, a significant improvement in the accuracy-robustness trade-off is achieved.

### 4.3. The mixing network

In practice, we use a neural network  $\alpha_\theta(\cdot) : \mathbb{R}^d \rightarrow [0, 1]$  to learn an effective mixing network that adjusts the outputs of  $g(\cdot)$  and  $h(\cdot)$ . Here,  $\theta$  represents the trainable parameters of the mixing network, and we refer to  $\alpha_\theta(\cdot)$  as the “mixing network”. To enforce an output range constraint, we apply a Sigmoid function to the mixing network. Note that when training the mixing network  $\alpha_\theta(\cdot)$ , the base classifiers  $g(\cdot)$  and  $h(\cdot)$  are frozen to avoid unnecessary feature distortions that the adversary can potentially exploit.

The mixing network’s task of treating clean and attacked inputs differently is closely related to the adversary detection problem. To this end, we adapt the detection architecture introduced in [56] for our mixing network. This architecture is end-to-end differentiable, making training and evaluation easier, and is also known for its performance and ease of implementation. While [20] has argued that simultaneously attacking the base classifier and the adversary detector can bring the detection rate of the detection method proposed in [56] to near zero, we show that with several key modifications, the method is effective even against strong white-box attacks. Specifically, our mixing network  $\alpha_\theta(\cdot)$  takes advantage of the two available models  $g(\cdot)$  and  $h(\cdot)$  by using the intermediate features of both networks via concatenation ([56] only has one base model). More importantly, we include stronger adaptive adversaries during training to generate much more diverse training examples.

The mixing network structure is based on a ResNet-18, which is known to perform well for a wide range of computer vision applications and is often considered the go-to architecture. We make minimum changes to the ResNet-18 to fit into our framework. As the mixing network takes information from both  $g(\cdot)$  and  $h(\cdot)$ , it uses the concatenated embeddings from the base classifiers. While [56] considers a single ResNet as the base classifier and uses the embeddings after the first ResNet block, to avoid the potential vulnerability against “feature adversaries” [66], we consider the embeddings from two different layers of the base model. Figure 3 demonstrates the modified architecture. The detailed implementations used in the experiment section are discussed in Appendix B.

Since Figure 1 shows that even a constant  $\alpha$  can alleviate the accuracy-robustness trade-off, our method does not excessively rely on the performance of the mixing network  $\alpha_\theta(\cdot)$ . In Section 5.3, we provide empirical results demonstrating that the above modifications help the overall mixed network defend against strong attacks.

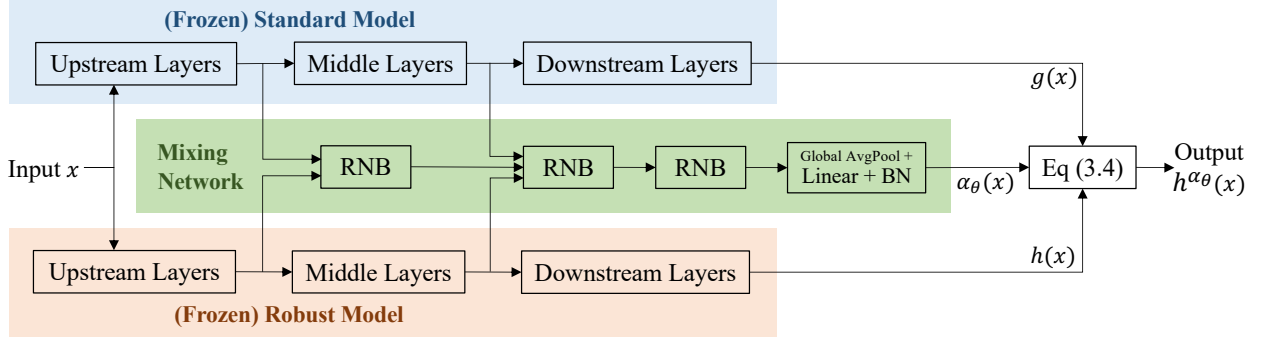


**Figure 3.** The overall architecture of the adaptively smoothed classifier introduced in Section 4. “RNB” stands for ResNetBlock and “BN” represents the 2D batch normalization layer.

#### 4.4. Training the mixing network

Consider the following two loss functions for training the mixing network  $\alpha_\theta(\cdot)$ :

- **Multi-class cross-entropy:** We minimize the multi-class cross-entropy loss of the combined classifier, which is the ultimate goal of the mixing network:

$$\min_{\theta} \mathbb{E}_{(x,y) \sim \mathcal{D}} \left[ \ell_{\text{CE}}(h^{\alpha_\theta}(x + \delta), y) \right], \quad (8)$$

where  $\ell_{\text{CE}}$  is the cross-entropy (CE) loss for logits and  $y \in [c]$  is the label corresponding to  $x$ . The base classifiers  $g(\cdot)$  and  $h(\cdot)$  are frozen and not updated. Again,  $\delta$  denotes the perturbation and the distribution  $\mathcal{F}$  is arbitrary. In our experiments, to avoid overfitting to a particular attack radius,  $\mathcal{F}$  is selected to be formed by perturbations with randomized radii.

- **Binary cross-entropy:** The optimal  $\alpha^*$  (parameterized by an optimal  $\theta^*$ ) that minimizes  $\ell_{\text{CE}}$  in (8) can be estimated for each training point. Specifically, depending on whether the input is attacked and how it is attacked, either  $g(\cdot)$  or  $h(\cdot)$  should be prioritized. Thus, we treat the task as a binary classification problem and solve the optimization problem

$$\min_{\theta} \mathbb{E}_{(x,y) \sim \mathcal{D}} \left[ \ell_{\text{BCE}}(\alpha_\theta(x + \delta), \tilde{\alpha}) \right],$$

where  $\ell_{\text{BCE}}$  is the binary cross-entropy (BCE) loss for probabilities and  $\tilde{\alpha} \in \{0, 1\}$  is the “pseudo label” for the output of the mixing network.

Using only the multi-class loss suffers from a distributional mismatch between the training set and the test set. The robust classifier  $h(\cdot)$  may achieve a low loss on adversarial training data but a high loss on adversarial test data. For example, with the CIFAR-10 dataset and our ResNet-18 robust classifier, the PGD<sub>10</sub> adversarial training accuracy is 93.01% while the PGD<sub>10</sub> test accuracy is 45.55%. As a result, approximating (8) with empirical risk minimization on the training set does not effectively optimize the true risk. When the adversary attacks a test input  $x$  targeting  $h(\cdot)$ , the standard prediction  $g(x)$  yields a lower loss than  $h(x)$ . However, if  $x$  is an attacked example in the



training set, then the losses of  $g(x)$  and  $h(x)$  are similar, and the mixing network does not receive a strong incentive to choose  $g(\cdot)$  when it detects an attack targeting  $h(\cdot)$ .

The binary loss, however, does not capture the potentially different sensitivity of each input. Certain inputs can be more vulnerable against adversarial attacks, and ensuring the correctness of the mixing network on these inputs is more crucial.

To this end, we propose a composite loss function that combines the above two components, providing incentives for the mixing network to select the standard classifier  $g(\cdot)$  when appropriate, while forcing the mixing network to remain conservative. The composite loss for a data-label pair  $(x, y)$  is given by

$$\begin{aligned} \ell_{\text{composite}}(\theta, (x, y, \tilde{\alpha})) = & c_{\text{CE}} \cdot \ell_{\text{CE}}(h^{\alpha_\theta}(x + \delta), y) + c_{\text{BCE}} \cdot \ell_{\text{BCE}}(\alpha_\theta(x + \delta), \tilde{\alpha}) \\ & + c_{\text{prod}} \cdot \ell_{\text{CE}}(h^{\alpha_\theta}(x + \delta), y) \cdot \ell_{\text{BCE}}(\alpha_\theta(x + \delta), \tilde{\alpha}), \end{aligned} \quad (9)$$

where the hyperparameters  $c_{\text{CE}}$ ,  $c_{\text{BCE}}$ , and  $c_{\text{prod}}$  control the weights of the loss components. In Appendix C, we discuss how these hyperparameters affect the performance of the trained mixing model.

## 5. Numerical experiments

### 5.1. Robust neural network smoothing with a fixed strength

We first consider the case where the smoothing strength  $\alpha$  is a fixed value, and use the CIFAR-10 dataset to evaluate the performance of the mixed classifier  $h^\alpha(\cdot)$  with various values of  $\alpha$ . Specifically, we use a ResNet18 model trained on clean data as the standard model  $g(\cdot)$  and use another ResNet18 trained on PGD<sub>20</sub> data as the robust model  $h(\cdot)$ . We consider PGD<sub>20</sub> attacks that target  $g(\cdot)$  and  $h(\cdot)$  individually (abbreviated as STD and ROB attacks), in addition to the adaptive PGD<sub>20</sub> attack generated using the end-to-end gradient of  $h^\alpha(\cdot)$ , denoted as the MIX attack.

The test accuracy of each mixed classifier is presented in Fig. 4. As  $\alpha$  increases, the clean accuracy of  $h^\alpha(\cdot)$  converges from the clean accuracy of  $g(\cdot)$  to the clean accuracy of  $h(\cdot)$ . In terms of the attacked performance, when the attack targets  $g(\cdot)$ , the attacked accuracy increases with  $\alpha$ . When the attack targets  $h(\cdot)$ , the attacked accuracy decreases with  $\alpha$ , showing that the attack targeting  $h(\cdot)$  becomes more benign when the mixed classifier emphasizes  $g(\cdot)$ . When the attack targets  $h^\alpha(\cdot)$ , the attacked accuracy increases with  $\alpha$ .

When  $\alpha$  is around 0.5, the MIX-attacked accuracy of  $h^\alpha(\cdot)$  quickly increases from near zero to more than 30% (which is two third of  $h(\cdot)$ 's attacked accuracy). This observation precisely matches the theoretical intuition provided by Theorem 1. On the other hand, when  $\alpha$  is greater than 0.5, the clean accuracy gradually decreases at a much slower rate, leading to the noticeably alleviated accuracy-robustness trade-off. Note that this improved trade-off is achieved without any further training beyond the weights of  $g(\cdot)$  and  $h(\cdot)$ .

This difference in how clean and attacked accuracies change with  $\alpha$  can be explained by the prediction confidence of  $h(\cdot)$ . Specifically, according to Table 1,  $h(\cdot)$  can make correct predictions under attack relatively confidently (average robustness margin is 0.768 with PGD<sub>20</sub> and 0.992 for AutoAttack). Thus, once  $\alpha$  becomes greater than 0.5 and gives  $h(\cdot)$  more authority over  $g(\cdot)$ ,  $h(\cdot)$  can use this confidence to correct  $g(\cdot)$ 's mistakes. On the other hand,  $h(\cdot)$  is unconfident when it produces incorrect predictions on clean data (the gap between the top two classes is only 0.434).

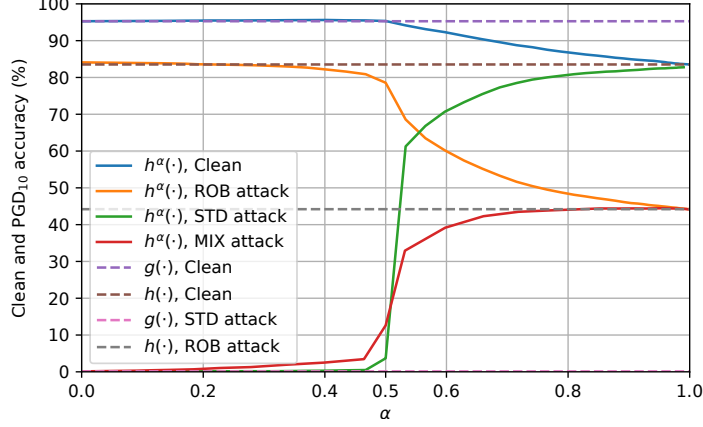


**Figure 4.** The performance of the mixed classifier  $h^\alpha(\cdot)$ . “STD attack”, “ROB attack”, and “MIX attack” refer to the PGD<sub>20</sub> attack generated using the gradient of  $g(\cdot)$ ,  $h(\cdot)$ , and  $h^\alpha(\cdot)$  respectively, with  $\epsilon$  set to  $8/255$ .

**Table 1.** Average gap between the probabilities of the predicted class and the runner-up class.  $g(\cdot)$  and  $h(\cdot)$  are the same ones used in Fig. 4. The confidence difference highlighted by the bold numbers is crucial to the mitigated accuracy-robustness trade-off of the mixed classifier.

	Clean			PGD <sub>20</sub>			AutoAttack		
	Accuracy	✓ Gap	✗ Gap	Accuracy	✓ Gap	✗ Gap	Accuracy	✓ Gap	✗ Gap
$g(\cdot)$	95.28%	0.982	0.698	0.10%	0.596	0.998	0.00%	—	0.986
$h(\cdot)$	83.53%	0.854	<b>0.434</b>	44.17%	<b>0.768</b>	0.635	40.80%	<b>0.992</b>	0.553

✓ Gap: The average margin between the confidences of the predicted class and the runner-up class among all correctly predicted validation data.

✗ Gap: The same quantity evaluated among all incorrectly predicted validation data.

In contrast,  $g(\cdot)$  is highly accurate and confident on clean data, but also makes confident mistakes when under attack. As a result, even when  $\alpha \geq 0.5$  and  $g(\cdot)$  is less powerful than  $h(\cdot)$ ,  $g(\cdot)$  can still correct some of the mistakes from  $h(\cdot)$  on clean data. This behavior in  $h(\cdot)$ ’s confidence is the key source of the improved accuracy-robustness trade-off. Additional analyses in Appendix A with more models show that this confidence property is shared by multiple robust classifiers.

Note that the average robust margin of  $h(\cdot)$  evaluated with AutoAttack (0.992) is much higher than that assessed with the weaker PGD<sub>20</sub> attack (0.768). This seemingly counterintuitive phenomenon is caused by the long-tailed distribution of the robust margins of  $h(\cdot)$ , which favors adaptive smoothing. Specifically, since the median robust margin evaluated with PGD<sub>20</sub> is 0.933, which is much larger than the 0.768 mean, we can conclude that most of the correctly predicted PGD<sub>20</sub> inputs have very large margins, and only a small portion suffer from small margins. These unconfidently predicted examples are, in fact, non-robust, and the stronger AutoAttack successfully changes their corresponding predictions. These results show that for a given validation input, if the robust base classifier  $h(\cdot)$  is robust at this input, it is highly likely to be robust with a large margin (i. e. far from the decision boundary). Such a property is precisely what adaptive smoothing relies

on, as shown in Lemma 1. On the other hand, the median confidence gap of  $h(\cdot)$  on incorrect clean data is 0.378 (the mean is 0.434), which implies that  $h(\cdot)$  is often unconfident when it makes mistakes, with the occurrence of confident incorrect predictions comparatively rare, again favoring the adaptive smoothing formulation.

## 5.2. Visualization of the Certified Robust Radii

Next, we visualize the certified robust radii presented in Theorem 1 and Theorem 2. In this subsection, the smoothing strength  $\alpha$  is again a fixed value. Since a (Gaussian) RS model with smoothing covariance matrix  $\sigma^2 I_d$  has an  $\ell_2$ -Lipschitz constant  $\sqrt{\frac{2}{\pi\sigma^2}}$ , such a model can be used to simultaneously visualize both theorems, with Theorem 2 giving tighter certificates of robustness. Note that RS models with a larger smoothing variance certify larger radii but achieve lower clean accuracies, and vice versa. Here, we consider the CIFAR-10 dataset and select  $g(\cdot)$  to be a ConvNeXT-T model with a clean accuracy of 97.25%, and use the RS models presented in [79] as  $h(\cdot)$ . For a fair comparison, we select an  $\alpha$  value such that the clean accuracy of the constructed mixed classifier  $h^\alpha(\cdot)$  matches that of another RS model  $h_{\text{baseline}}(\cdot)$  with a smaller smoothing variance. The expectation term in the RS formulation is approximated with the empirical mean of 10000 random perturbations drawn from  $\mathcal{N}(0, \sigma^2 I_d)$ , and the certified radii of  $h_{\text{baseline}}(\cdot)$  are calculated using Theorems 1 and 2 by setting  $\alpha$  to 1. Fig. 5 displays the calculated certified accuracies of  $h^\alpha(\cdot)$  and  $h_{\text{baseline}}(\cdot)$  at various attack radii. The ordinate ‘‘Accuracy’’ at a given abscissa ‘‘ $\ell_2$  radius’’ reflects the percentage of the test data for which the considered model gives a correct prediction as well as a certified radius at least as large as the  $\ell_2$  radius under consideration.

In both subplots of Fig. 5, the certified robustness curves of  $h^\alpha(\cdot)$  do not connect to the clean accuracy when  $\alpha$  approaches zero. This is because Theorems 1 and 2 both consider robustness with respect to  $h(\cdot)$  and do not issue certificates to test inputs at which  $h(\cdot)$  makes incorrect predictions, even if  $h^\alpha(\cdot)$  predicts correctly at some of these points. This is reasonable because we do not assume any robustness or Lipschitzness of  $g(\cdot)$ , and  $g(\cdot)$  is allowed to be arbitrarily incorrect whenever the radius is non-zero.

The Lipschitz-based bound of Theorem 1 allows us to visualize the performance of the mixed classifier  $h^\alpha(\cdot)$  when  $h(\cdot)$  is an  $\ell_2$ -Lipschitz model. In this case, the curves associated with  $h^\alpha(\cdot)$  and  $h_{\text{baseline}}(\cdot)$  intersect, with  $h^\alpha(\cdot)$  achieving higher certified accuracy at larger radii and  $h_{\text{baseline}}(\cdot)$  certifying more points at smaller radii. By adjusting  $\alpha$  and the Lipschitz constant of  $h(\cdot)$ , it is possible to change the location of this intersection while maintaining the same level of clean accuracy. Therefore, the mixed classifier structure allows for optimizing the certified accuracy at a particular radius, while keeping the clean accuracy unchanged.

The RS-based bound from Theorem 2 captures the behavior of  $h^\alpha(\cdot)$  when  $h(\cdot)$  is an RS model. For both  $h^\alpha(\cdot)$  and  $h_{\text{baseline}}(\cdot)$ , the RS-based bounds certify larger radii than the corresponding Lipschitz-based bounds. Nonetheless,  $h_{\text{baseline}}(\cdot)$  can certify more points with the RS-based guarantee. Intuitively, this phenomenon suggests that RS models can yield correct but low-confidence predictions when under attack with a large radius, and thus may not be best-suited for our mixing operation, which relies on robustness with non-zero margins. In contrast, Lipschitz models, a more general and common class of models, exploit the mixing operation more effectively. Moreover, as shown in Fig. 4, empirically robust models often yield high-confidence predictions when under attack, making them more suitable to be used as the robust base classifier for  $h^\alpha(\cdot)$ .

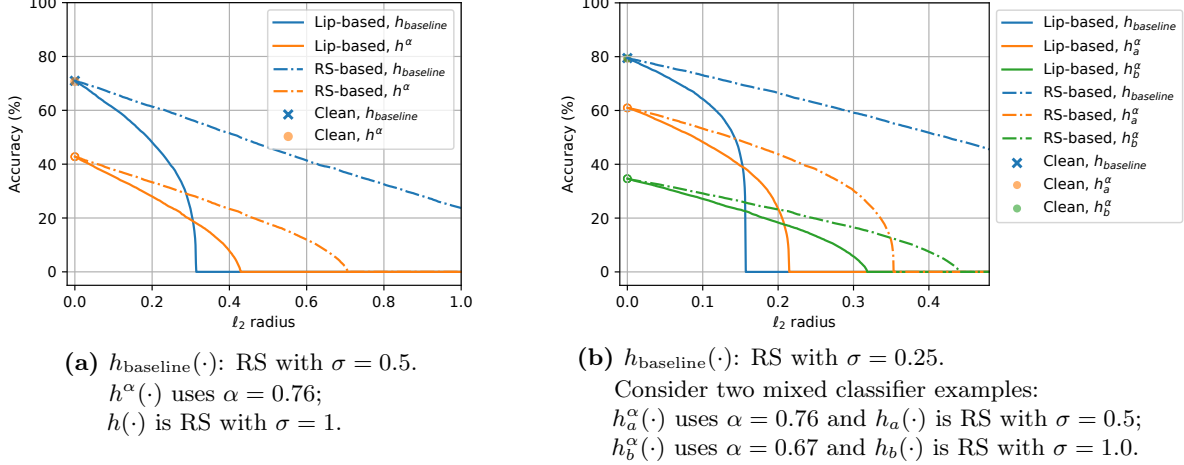


**Figure 5.** Comparing the certified accuracy-robustness trade-off of RS models and our mixed classifier using both Lipschitz-based (Lip-based) certificates and RS-based certificates (Theorems 1 and 2, respectively). The clean accuracies are the same between  $h_{\text{baseline}}(\cdot)$  and  $h^\alpha(\cdot)$  in each subfigure, and the empty circles represent discontinuity in the certified accuracy at radius 0.

### 5.3. Robust neural network smoothing with adaptive strength

Having validated the effectiveness of the mixing formulation described in (4), we are now ready to incorporate the mixing network for adaptive smoothing strength into the empirical analyses. As in Section 4, we denote the parameterized mixing network by  $\alpha_\theta(\cdot)$ , and we slightly abuse notation by denoting the composite classifier with adaptive smoothing strength given by  $\alpha_\theta(\cdot)$  by  $h^{\alpha_\theta}(\cdot)$ , which is defined by  $h^{\alpha_\theta}(x) = h^{\alpha_\theta(x)}(x)$ .

CIFAR-10 and CIFAR-100 are two of the most widely used benchmark datasets for evaluating adversarial robustness. Although recent progress in learning robust models has made the accuracy-robustness trade-off less noticeable for the easier CIFAR-10 dataset, with robust neural networks almost matching standard models on clean accuracy [35, 36, 65], the trade-off remains highly noticeable for more challenging tasks such as CIFAR-100, for which robust models suffer from significant accuracy degradation. As existing methods for improving standard model performance may not readily extend to robust models, mixing pre-trained classifiers via adaptive smoothing becomes particularly advantageous for these harder tasks.

In this section, we use small CIFAR-10 models to perform ablation analyses and proof-of-concept demonstrations. For the more challenging CIFAR-100 dataset, we use state-of-the-art classifiers as base models, with  $g(\cdot)$  taking advantage of accuracy-optimized pre-training and  $h(\cdot)$  exploiting recent robust training methods. We then apply adaptive smoothing to these high-performance models and demonstrate that our method produces models that are both accurate and robust, reconciling the accuracy-robustness trade-off to an unprecedented level.

#### 5.3.1 Proof-of-concept demonstrations with CIFAR-10

In all experiments, we consider  $\ell_\infty$  attacks and use the AdamW optimizer [44] for optimization. Appendix B discusses the details of implementing the architecture shown in Figure 3 for the experi-

**Table 2.** CIFAR-10 results of the adaptively smoothed models trained with three different settings.

CIFAR-10 base classifier performances				
Model	Architecture	Clean	PGD <sub>20</sub>	AutoAttack
$g(\cdot)$ (accurate)	ResNet-18 (Standard non-robust training)	95.28 %	0.12 %	0.00 %
$h(\cdot)$ (robust)	WideResNet-34 (TRADES model from [79])	84.92 %	57.16 %	53.09 %

CIFAR-10 adaptive smoothing $h^{\alpha_\theta}(\cdot)$ performance			
Evaluation Data \ Training Setting	A	B	C
Clean	92.05 %	92.07 %	91.51 %
<b>A</b> (gray-box PGD <sub>20</sub> )	57.22 %	57.25 %	56.30 %
<b>B</b> (white-box PGD <sub>20</sub> )	56.63 %	57.09 %	56.29 %
<b>C</b> (white-box AutoAttack)	40.04 %	40.02 %	42.78 %
<b>D</b> (adaptive AutoAttack)	39.85 %	39.70 %	42.66 %

ments. The training inputs for the mixing network  $\alpha_\theta(\cdot)$  include the clean data and the corresponding types of attacked data (attack settings A, B, and C presented in Section 4.2). For the setting C (AutoAttack), the training data only include targeted and untargeted APGD attacks, with the other two AutoAttack components, FAB and Square, excluded during training in the interest of efficiency but are included for evaluation. To alleviate overfitting, we randomize the attack radius and the number of steps. Moreover, when generating training-time attacks, we add a randomly-weighted binary cross-entropy loss component that targets the mixing network (this loss tries to trick the mixing network to favor  $g(\cdot)$ ). In Appendix C, we perform an ablation study on the hyperparameters of the composite loss function (9).

Table 2 gives the validation accuracy of  $h^{\alpha_\theta}(\cdot)$  for each setting, where each column represents the performance of one adaptively smoothed model. The results show that the combined classifier can defend against the attacks it is trained on.

Specifically, for the attack setting A (gray-box PGD),  $h^{\alpha_\theta}(\cdot)$  is able to achieve the same level of PGD<sub>20</sub>-attacked accuracy as  $h(\cdot)$  while retaining a similar level of clean accuracy as  $g(\cdot)$ . For the setting B (white-box PGD), the attack is allowed to follow the gradient path provided by  $\alpha_\theta(\cdot)$  and deliberately evade the part of the adversarial input space recognized by  $\alpha_\theta(\cdot)$ . While the training task becomes more challenging, the improvement in the accuracy-robustness trade-off is still substantial. Furthermore, the composite model can generalize to examples generated via the stronger AutoAttack. For the setting C (AutoAttack), the difficulty of the training problem further escalates. While the performance of  $h^{\alpha_\theta}(\cdot)$  on clean data slightly decreases, the mixing network can offer a more vigorous defense against AutoAttack data, still improving the accuracy-robustness trade-off.

As discussed earlier, adaptive smoothing is particularly advantageous for more challenging tasks where the accuracy-robustness trade-off is highly noticeable. As a result, its advantages over existing methods may not be immediately apparent on easier datasets such as CIFAR-10. In the next section, we demonstrate competitive results on the harder CIFAR-100 dataset.

**Table 3.** CIFAR-100 results of the adaptively smoothed models trained with the three settings. When the training setting C is used, an 80.90% clean accuracy and a 32.94% AutoAttacked accuracy is achieved.

CIFAR-100 base classifier performances				
Model	Architecture	Clean	PGD <sub>20</sub>	AutoAttack
$g(\cdot)$ (accurate)	ResNet-152 (Based on BiT [45])	91.38 %	0.14 %	0.00 %
$h(\cdot)$ (robust)	WideResNet-70 (From [35])	69.17 %	40.86 %	36.98 %

CIFAR-100 adaptive smoothing $h^{\alpha_\theta}(\cdot)$ performance			
Evaluation Data \ Training Setting	A	B	C
Clean	83.99 %	83.96 %	80.90 %
<b>A</b> (gray-box PGD <sub>20</sub> )	40.04 %	39.80 %	39.26 %
<b>B</b> (white-box PGD <sub>20</sub> )	30.59 %	34.48 %	38.92 %
<b>C</b> (white-box AutoAttack)	23.54 %	26.37 %	32.94 %
<b>D</b> (adaptive AutoAttack)	23.78 %	26.17 %	32.80 %

### 5.3.2 Improved accuracy-robustness trade-off on CIFAR-100

In this section, we repeat the above experiments with state-of-the-art CIFAR-100 classifiers, with the results displayed in Table 3. We also include comparisons with existing robust training methods, especially those aiming to alleviate the accuracy-robustness trade-off, in Table 4.

The results in Table 3 confirm that adaptive smoothing achieves even more significant improvements on the CIFAR-100 dataset. Notably, even for the most challenging attack setting C,  $h^{\alpha_\theta}(\cdot)$  correctly classifies 1173 additional clean images compared with  $h(\cdot)$  (cutting the error rate by a third) while making only 404 additional incorrect predictions on AutoAttacked inputs (increasing the error rate by merely 6.4 relative percent). Such results show that  $\alpha_\theta(\cdot)$  is capable of approximating a robust high-performance mixing network when trained with sufficiently diverse attacked data. The fact that  $h^{\alpha_\theta}(\cdot)$  combines the clean accuracy of  $g(\cdot)$  and the robustness of  $h(\cdot)$  highlights that our method significantly improves the accuracy-robustness trade-off.

Next, in Table 4, we compare these results with existing methods. Since the literature has generally regarded AutoAttack as one of the most reliable and appropriate robustness evaluation methods (weaker attacks such as PGD are easily circumventable), we select existing works that use AutoAttack as the benchmark. We implement adaptive smoothing using two different robust base classifiers, with the aforementioned BiT [45] ResNet-152 selected as the accurate base model for both cases. We highlight that the listed works should not be treated as competitors, since advancements in building robust classifiers can be incorporated into our framework as  $h(\cdot)$ , helping adaptive smoothing perform even better.

The results in Table 4 demonstrate that compared with their corresponding robust base models, both implementations of adaptive smoothing improve the clean accuracy by ten percentage points, with the AutoAttacked accuracy only deteriorating by four percentage points. Notably, as of the submission of this paper, on the CIFAR-100 dataset, the composite classifier based on the robust model introduced in [76] achieves an AutoAttacked accuracy better than any other methods listed on RobustBench [26], with the exception of [76] itself. Simultaneously, this mixed model offers an improvement of ten percentage points compared with any other listed models. These results demonstrate that adaptive smoothing significantly alleviates the accuracy-robustness trade-off of



**Table 4.** The clean and AutoAttacked accuracy of adaptive smoothing on CIFAR-100 compared with existing works.

Method	Model Architecture	Clean	AutoAttack
Adaptive Smoothing (this work)**	ResNet-152 + WRN-70-16	85.21 %	38.72 %
Adaptive Smoothing (this work)*	ResNet-152 + WRN-70-16	80.90 %	32.94 %
Diffusion (EDM) + TRADES <sup>‡</sup> [76]	WideResNet-70-16	75.22 %	42.67 %
Unlabeled data + TRADES <sup>†</sup> [35]	WideResNet-70-16	69.17 %	36.98 %
TRADES <sup>‡</sup> [30]	XCiT-L12 [6]	70.76 %	35.08 %
Diffusion (DDPM) + TRADES <sup>‡</sup> [65]	WideResNet-70-16	63.56 %	34.64 %
SCORE Loss AT <sup>‡</sup> [60]	WideResNet-70-16	65.56 %	33.05 %
Diffusion (DDPM) + AT <sup>‡</sup> [69]	WideResNet-34-10	65.93 %	31.15 %
TRADES <sup>‡</sup> [35]	WideResNet-70-16	60.86 %	30.03 %

\*: Uses “Unlabeled data + TRADES” [35] as the robust base model  $h(\cdot)$ .

\*\* : Uses “EDM + TRADES” [76] as the robust base model  $h(\cdot)$ .

<sup>†</sup>: Model provided by the authors evaluated by us.    <sup>‡</sup>: Reported by the authors.

neural classifiers.

## 6. Conclusions

This paper proposes “adaptive smoothing”, a flexible framework that leverages the mixture of the probability outputs of an accurate model and a robust model to mitigate the accuracy-robustness trade-off of neural classifiers. We mathematically prove that the smoothed composite model can inherit the certified robustness of the robust base model under realistic assumptions. We then adapt an adversarial input detector into a (deterministic) mixing network, further improving the accuracy-robustness trade-off. Solid empirical results confirm that our method can simultaneously benefit from the high accuracy of modern pre-trained standard (non-robust) models and the robustness achieved via state-of-the-art robust classification methods.

Because our theoretical study demonstrates the possibility of leveraging the mixing network to avoid the accuracy-robustness trade-off entirely, future advancements in adversarial example identification can reconcile this trade-off even more effectively via our framework. Furthermore, the proposed method can be conveniently extended to various attack types and budgets. Thus, this work paves the way for future research to focus on either accuracy or robustness without sacrificing the other.

## References

- [1] George Adam and Romain Speciel. Evaluating ensemble robustness against adversarial attacks. *arXiv preprint arXiv:2005.05750*, 2020.
- [2] Morteza Ali Ahmadi, Rouhollah Dianat, and Hossein Amirkhani. An adversarial attack detection method in deep neural networks based on re-attacking approach. *Multimedia Tools and Applications*, 80(7):10985–11014, 2021.
- [3] Manaar Alam, Shubhajit Datta, Debdeep Mukhopadhyay, Arijit Mondal, and Partha Pra-

- tim Chakrabarti. Resisting adversarial attacks in deep neural networks using diverse decision boundaries. *arXiv preprint arXiv:2208.08697*, 2022.
- [4] Ahmed Aldahdooh, Wassim Hamidouche, and Olivier Déforges. Selective and features based adversarial example detection. *arXiv preprint arXiv:2103.05354*, 2021.
  - [5] Ahmed Aldahdooh, Wassim Hamidouche, Sid Ahmed Fezza, and Olivier Déforges. Adversarial example detection for dnn models: A review and experimental comparison. *arXiv preprint arXiv:2105.00203*, 2021.
  - [6] Alaaeldin Ali, Hugo Touvron, Mathilde Caron, Piotr Bojanowski, Matthijs Douze, Armand Joulin, Ivan Laptev, Natalia Neverova, Gabriel Synnaeve, Jakob Verbeek, et al. Xcit: Cross-covariance image transformers. In *Advances in neural information processing systems*, 2021.
  - [7] Brendon G. Anderson, Ziyi Ma, Jingqi Li, and Somayeh Sojoudi. Tightened convex relaxations for neural network robustness certification. In *IEEE Conference on Decision and Control*, 2020.
  - [8] Brendon G Anderson and Somayeh Sojoudi. Certified robustness via locally biased randomized smoothing. In *Annual Learning for Dynamics and Control Conference*, 2022.
  - [9] Brendon G Anderson and Somayeh Sojoudi. Data-driven certification of neural networks with random input noise. *IEEE Transactions on Control of Network Systems*, 2022.
  - [10] Maksym Andriushchenko, Francesco Croce, Nicolas Flammarion, and Matthias Hein. Square attack: A query-efficient black-box adversarial attack via random search. In *European Conference on Computer Vision*, 2020.
  - [11] Anish Athalye, Nicholas Carlini, and David Wagner. Obfuscated gradients give a false sense of security: Circumventing defenses to adversarial examples. In *International Conference on Machine Learning*, 2018.
  - [12] Anish Athalye, Logan Engstrom, Andrew Ilyas, and Kevin Kwok. Synthesizing robust adversarial examples. In *International Conference on Machine Learning*, 2018.
  - [13] Tao Bai, Jinqi Luo, Jun Zhao, Bihan Wen, and Qian Wang. Recent advances in adversarial training for adversarial robustness. In *International Joint Conference on Artificial Intelligence*, 2021.
  - [14] Yatong Bai, Brendon G Anderson, and Somayeh Sojoudi. Mixing classifiers to alleviate the accuracy-robustness trade-off. [https://bai-yt.github.io/files/publications/MixedClassifier\\_PrePrint.pdf](https://bai-yt.github.io/files/publications/MixedClassifier_PrePrint.pdf), 2023. Submitted for conference publication.
  - [15] Yatong Bai, Tanmay Gautam, Yu Gai, and Somayeh Sojoudi. Practical convex formulation of robust one-hidden-layer neural network training. In *American Control Conference*, 2022.
  - [16] Yatong Bai, Tanmay Gautam, and Somayeh Sojoudi. Efficient global optimization of two-layer relu networks: Quadratic-time algorithms and adversarial training. *SIAM Journal on Mathematics of Data Science*, 2022.
  - [17] Yogesh Balaji, Tom Goldstein, and Judy Hoffman. Instance adaptive adversarial training: Improved accuracy tradeoffs in neural nets. *arXiv preprint arXiv:1910.08051*, 2019.

- [18] Jaydeep Borkar and Pin-Yu Chen. Simple transparent adversarial examples. *arXiv preprint arXiv:2105.09685*, 2021.
- [19] Nicholas Carlini, Florian Tramer, J Zico Kolter, et al. (certified!!) adversarial robustness for free! *arXiv preprint arXiv:2206.10550*, 2022.
- [20] Nicholas Carlini and David Wagner. Adversarial examples are not easily detected: Bypassing ten detection methods. In *ACM Workshop on Artificial Intelligence and Security*, 2017.
- [21] Nicholas Carlini and David A. Wagner. Towards evaluating the robustness of neural networks. In *IEEE Symposium on Security and Privacy*, 2017.
- [22] Fabio Carrara, Fabrizio Falchi, Roberto Caldelli, Giuseppe Amato, and Rudy Becarelli. Adversarial image detection in deep neural networks. *Multimedia Tools and Applications*, 78(3):2815–2835, 2019.
- [23] Tianlong Chen, Sijia Liu, Shiyu Chang, Yu Cheng, Lisa Amini, and Zhangyang Wang. Adversarial robustness: From self-supervised pre-training to fine-tuning. In *The IEEE/CVF Conference on Computer Vision and Pattern Recognition*, 2020.
- [24] Kenneth T Co, David Martinez-Rego, Zhongyuan Hau, and Emil C Lupu. Jacobian ensembles improve robustness trade-offs to adversarial attacks. In *Artificial Neural Networks and Machine Learning*, 2022.
- [25] Jeremy Cohen, Elan Rosenfeld, and Zico Kolter. Certified adversarial robustness via randomized smoothing. In *International Conference on Machine Learning*, 2019.
- [26] Francesco Croce, Maksym Andriushchenko, Vikash Sehwal, Edoardo Debenedetti, Nicolas Flammarion, Mung Chiang, Prateek Mittal, and Matthias Hein. Robustbench: a standardized adversarial robustness benchmark. *arXiv preprint arXiv:2010.09670*, 2020.
- [27] Francesco Croce, Sven Gowal, Thomas Brunner, Evan Shelhamer, Matthias Hein, and Taylan Cemgil. Evaluating the adversarial robustness of adaptive test-time defenses. *arXiv preprint arXiv:2202.13711*, 2022.
- [28] Francesco Croce and Matthias Hein. Minimally distorted adversarial examples with a fast adaptive boundary attack. In *International Conference on Machine Learning*, 2020.
- [29] Francesco Croce and Matthias Hein. Reliable evaluation of adversarial robustness with an ensemble of diverse parameter-free attacks. In *International Conference on Machine Learning*, 2020.
- [30] Edoardo Debenedetti, Vikash Sehwal, and Prateek Mittal. A light recipe to train robust vision transformers. *arXiv preprint arXiv:2209.07399*, 2022.
- [31] Lijie Fan, Sijia Liu, Pin-Yu Chen, Gaoyuan Zhang, and Chuang Gan. When does contrastive learning preserve adversarial robustness from pretraining to finetuning? In *Annual Conference on Neural Information Processing Systems*, 2021.

- [32] Mahyar Fazlyab, Alexander Robey, Hamed Hassani, Manfred Morari, and George Pappas. Efficient and accurate estimation of lipschitz constants for deep neural networks. In *Annual Conference on Neural Information Processing Systems*, 2019.
- [33] Ivan Fursov, Alexey Zaytsev, Pavel Burnyshev, Ekaterina Dmitrieva, Nikita Klyuchnikov, Andrey Kravchenko, Ekaterina Artemova, Evgenia Komleva, and Evgeny Burnaev. A differentiable language model adversarial attack on text classifiers. *IEEE Access*, 10:17966–17976, 2022.
- [34] Ian J. Goodfellow, Jonathon Shlens, and Christian Szegedy. Explaining and harnessing adversarial examples. In *International Conference on Learning Representations*, 2015.
- [35] Sven Gowal, Chongli Qin, Jonathan Uesato, Timothy Mann, and Pushmeet Kohli. Uncovering the limits of adversarial training against norm-bounded adversarial examples. *arXiv preprint arXiv:2010.03593*, 2020.
- [36] Sven Gowal, Sylvestre-Alvise Rebuffi, Olivia Wiles, Florian Stimberg, Dan A. Calian, and Timothy Mann. Improving robustness using generated data. *arXiv preprint arXiv:2110.09468*, 2021.
- [37] Sven Gowal, Jonathan Uesato, Chongli Qin, Po-Sen Huang, Timothy Mann, and Pushmeet Kohli. An alternative surrogate loss for pgd-based adversarial testing. *arXiv preprint arXiv:1910.09338*, 2019.
- [38] Kaiming He, Xiangyu Zhang, Shaoqing Ren, and Jian Sun. Deep residual learning for image recognition. In *IEEE conference on computer vision and pattern recognition*, 2016.
- [39] Matthias Hein and Maksym Andriushchenko. Formal guarantees on the robustness of a classifier against adversarial manipulation. In *Annual Conference on Neural Information Processing Systems*, 2017.
- [40] Ting-Kuei Hu, Tianlong Chen, Haotao Wang, and Zhangyang Wang. Triple wins: Boosting accuracy, robustness and efficiency together by enabling input-adaptive inference. In *International Conference on Learning Representations*, 2020.
- [41] Sandy H. Huang, Nicolas Papernot, Ian J. Goodfellow, Yan Duan, and Pieter Abbeel. Adversarial attacks on neural network policies. In *International Conference on Learning Representations*, 2017.
- [42] Andrew Ilyas, Logan Engstrom, Anish Athalye, and Jessy Lin. Black-box adversarial attacks with limited queries and information. In *International Conference on Machine Learning*, 2018.
- [43] Xiaojun Jia, Yong Zhang, Baoyuan Wu, Ke Ma, Jue Wang, and Xiaochun Cao. LAS-AT: Adversarial training with learnable attack strategy. In *The IEEE/CVF Conference on Computer Vision and Pattern Recognition*, 2022.
- [44] Diederik P. Kingma and Jimmy Ba. Adam: A method for stochastic optimization. In *International Conference on Learning Representations*, 2015.

- [45] Alexander Kolesnikov, Lucas Beyer, Xiaohua Zhai, Joan Puigcerver, Jessica Yung, Sylvain Gelly, and Neil Houlsby. Big transfer (BiT): General visual representation learning. In *European Conference on Computer Vision*, 2020.
- [46] Alex Krizhevsky. Learning multiple layers of features from tiny images. <https://www.cs.toronto.edu/~kriz/learning-features-2009-TR.pdf>, 2012.
- [47] Alexey Kurakin, Ian J. Goodfellow, and Samy Bengio. Adversarial machine learning at scale. In *International Conference on Learning Representations*, 2017.
- [48] Alex Lamb, Vikas Verma, Juho Kannala, and Yoshua Bengio. Interpolated adversarial training: Achieving robust neural networks without sacrificing too much accuracy. In *ACM Workshop on Artificial Intelligence and Security*, 2019.
- [49] Alexander Levine, Sahil Singla, and Soheil Feizi. Certifiably robust interpretation in deep learning. *arXiv preprint arXiv:1905.12105*, 2019.
- [50] Bai Li, Changyou Chen, Wenlin Wang, and Lawrence Carin. Certified adversarial robustness with additive noise. In *Annual Conference on Neural Information Processing Systems*, 2019.
- [51] Chang Liu, Yinpeng Dong, Wenzhao Xiang, Xiao Yang, Hang Su, Jun Zhu, Yuefeng Chen, Yuan He, Hui Xue, and Shibao Zheng. A comprehensive study on robustness of image classification models: Benchmarking and rethinking. *arXiv preprint arXiv:2302.14301*, 2023.
- [52] Xuanqing Liu, Minhao Cheng, Huan Zhang, and Cho-Jui Hsieh. Towards robust neural networks via random self-ensemble. In *European Conference on Computer Vision*, 2018.
- [53] Zhuang Liu, Hanzi Mao, Chao-Yuan Wu, Christoph Feichtenhofer, Trevor Darrell, and Saining Xie. A convnet for the 2020s. In *The IEEE/CVF Conference on Computer Vision and Pattern Recognition*, 2022.
- [54] Ziyi Ma and Somayeh Sojoudi. A sequential framework towards an exact SDP verification of neural networks. In *International Conference on Data Science and Advanced Analytics*, 2021.
- [55] Aleksander Madry, Aleksandar Makelov, Ludwig Schmidt, Dimitris Tsipras, and Adrian Vladu. Towards deep learning models resistant to adversarial attacks. In *International Conference on Learning Representations*, 2018.
- [56] Jan Hendrik Metzen, Tim Genewein, Volker Fischer, and Bastian Bischoff. On detecting adversarial perturbations. In *International Conference on Learning Representations*, 2017.
- [57] Seyed-Mohsen Moosavi-Dezfooli, Alhussein Fawzi, and Pascal Frossard. Deepfool: A simple and accurate method to fool deep neural networks. In *IEEE Conference on Computer Vision and Pattern Recognition*, 2016.
- [58] Dongbin Na. Pytorch adversarial training on cifar-10. <https://github.com/ndb796/Pytorch-Adversarial-Training-CIFAR>, 2020.
- [59] Matteo Pagliardini, Gilberto Manunza, Martin Jaggi, and Tatjana Chavdarova. Improved generalization-robustness trade-off via uncertainty targeted attacks. Preprint, 2022.

- [60] Tianyu Pang, Min Lin, Xiao Yang, Jun Zhu, and Shuicheng Yan. Robustness and accuracy could be reconcilable by (proper) definition. *arXiv preprint arXiv:2202.10103*, 2022.
- [61] Tianyu Pang, Kun Xu, Chao Du, Ning Chen, and Jun Zhu. Improving adversarial robustness via promoting ensemble diversity. In *International Conference on Machine Learning*, 2019.
- [62] Nicolas Papernot, Patrick McDaniel, Ian Goodfellow, Somesh Jha, Z Berkay Celik, and Ananthram Swami. Practical black-box attacks against machine learning. In *ACM Asia Conference on Computer and Communications Security*, 2017.
- [63] Samuel Pfrommer, Brendon G Anderson, and Somayeh Sojoudi. Projected randomized smoothing for certified adversarial robustness. Preprint. <https://people.eecs.berkeley.edu/~sojoudi/pfrommer2022projected.pdf>, 2022.
- [64] Aditi Raghunathan, Sang Michael Xie, Fanny Yang, John C. Duchi, and Percy Liang. Understanding and mitigating the tradeoff between robustness and accuracy. In *International Conference on Machine Learning*, 2020.
- [65] Sylvestre-Alvise Rebuffi, Sven Gowal, Dan A Calian, Florian Stimberg, Olivia Wiles, and Timothy Mann. Fixing data augmentation to improve adversarial robustness. *arXiv preprint arXiv:2103.01946*, 2021.
- [66] Sara Sabour, Yanshuai Cao, Fartash Faghri, and David J Fleet. Adversarial manipulation of deep representations. *arXiv preprint arXiv:1511.05122*, 2015.
- [67] Hadi Salman, Jerry Li, Ilya Razenshteyn, Pengchuan Zhang, Huan Zhang, Sebastien Bubeck, and Greg Yang. Provably robust deep learning via adversarially trained smoothed classifiers. In *Annual Conference on Neural Information Processing Systems*, 2019.
- [68] Ludwig Schmidt, Shibani Santurkar, Dimitris Tsipras, Kunal Talwar, and Aleksander Madry. Adversarially robust generalization requires more data. In *Annual Conference on Neural Information Processing Systems*, 2018.
- [69] Vikash Sehwal, Saeed Mahloujifar, Tinashe Handina, Sihui Dai, Chong Xiang, Mung Chiang, and Prateek Mittal. Robust learning meets generative models: Can proxy distributions improve adversarial robustness? In *International Conference on Learning Representations*, 2022.
- [70] Ali Shafahi, Mahyar Najibi, Mohammad Amin Ghiasi, Zheng Xu, John Dickerson, Christoph Studer, Larry S Davis, Gavin Taylor, and Tom Goldstein. Adversarial training for free! In *Annual Conference on Neural Information Processing Systems*, 2019.
- [71] Florian Tramèr, Nicholas Carlini, Wieland Brendel, and Aleksander Madry. On adaptive attacks to adversarial example defenses. In *Annual Conference on Neural Information Processing Systems*, 2020.
- [72] Florian Tramèr, Alexey Kurakin, Nicolas Papernot, Ian J. Goodfellow, Dan Boneh, and Patrick D. McDaniel. Ensemble adversarial training: Attacks and defenses. In *International Conference on Learning Representations*, 2018.



- [73] Dimitris Tsipras, Shibani Santurkar, Logan Engstrom, Alexander Turner, and Aleksander Madry. Robustness may be at odds with accuracy. In *International Conference on Learning Representations*, 2019.
- [74] Haotao Wang, Tianlong Chen, Shupeng Gui, TingKuei Hu, Ji Liu, and Zhangyang Wang. Once-for-all adversarial training: In-situ tradeoff between robustness and accuracy for free. In *Annual Conference on Neural Information Processing Systems*, 2020.
- [75] Jianyu Wang and Haichao Zhang. Bilateral adversarial training: Towards fast training of more robust models against adversarial attacks. In *International Conference on Computer Vision*, 2019.
- [76] Zekai Wang, Tianyu Pang, Chao Du, Min Lin, Weiwei Liu, and Shuicheng Yan. Better diffusion models further improve adversarial training. *arXiv preprint arXiv:2302.04638*, 2023.
- [77] Yao-Yuan Yang, Cyrus Rashtchian, Hongyang Zhang, Russ R. Salakhutdinov, and Kamalika Chaudhuri. A closer look at accuracy vs. robustness. In *Annual Conference on Neural Information Processing Systems*, 2020.
- [78] Haichao Zhang and Jianyu Wang. Defense against adversarial attacks using feature scattering-based adversarial training. In *Annual Conference on Neural Information Processing Systems*, 2019.
- [79] Hongyang Zhang, Yaodong Yu, Jiantao Jiao, Eric P. Xing, Laurent El Ghaoui, and Michael I. Jordan. Theoretically principled trade-off between robustness and accuracy. In *International Conference on Machine Learning*, 2019.
- [80] Haizhong Zheng, Ziqi Zhang, Juncheng Gu, Honglak Lee, and Atul Prakash. Efficient adversarial training with transferable adversarial examples. In *The IEEE/CVF Conference on Computer Vision and Pattern Recognition*, 2020.
- [81] Yaowei Zheng, Richong Zhang, and Yongyi Mao. Regularizing neural networks via adversarial model perturbation. In *The IEEE/CVF Conference on Computer Vision and Pattern Recognition*, 2021.

## A. Additional empirical supports for selecting $R_i(x) = 1$

In this section, we use additional empirical evidence (Figures 6a and 6b) to show that  $R_i(x) = 1$  is the appropriate choice for the adaptive smoothing formulation, and that the post-SoftMax probabilities should be used for smoothing. While most of the experiments in this paper are based on ResNets, the architecture is chosen solely because of its popularity, and our method does not depend on any properties of ResNets. Therefore, for the experiment in Figure 6a, we select an alternative architecture by using a more modern ConvNeXT-T model [53] pre-trained on ImageNet-1k as  $g(\cdot)$ . We also use a robust model trained via TRADES in place of an adversarially-trained network for  $h(\cdot)$ . Moreover, while most of our experiments are based on  $\ell_\infty$  attacks, our method applies to all  $\ell_p$  attack budgets. In Figure 6b, we provide an example that considers the  $\ell_2$  attack. The experiment settings are summarized in Table 5.

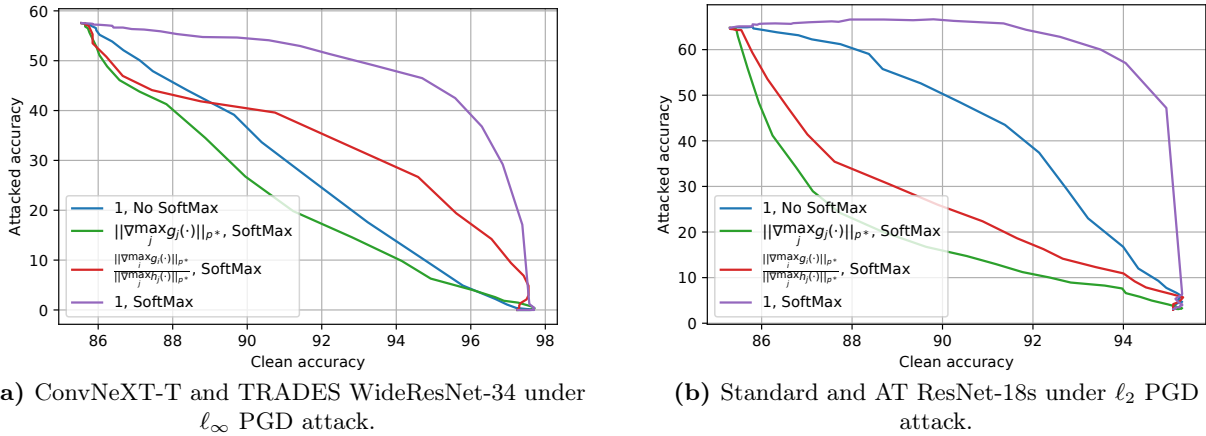


**Figure 6.** Comparing the “attacked accuracy versus clean accuracy” curve of various options for  $R_i(x)$  with alternative selections of base classifiers.

**Table 5.** Experiment settings for comparing the choices of  $R_i(x)$ .

	PGD attack settings	$g(\cdot)$ Architecture	$h(\cdot)$ Architecture
Figure 1	$\ell_\infty$ , $\epsilon = 8/255$ , 10 Steps	Standard ResNet-18	$\ell_\infty$ -adversarially-trained ResNet-18
Figure 6a	$\ell_\infty$ , $\epsilon = 8/255$ , 20 Steps	Standard ConvNeXT-T	TRADES WideResNet-34
Figure 6b	$\ell_2$ , $\epsilon = 0.5$ , 20 Steps	Standard ResNet-18	$\ell_2$ -adversarially-trained ResNet-18

Figures 6a and 6b demonstrate that setting  $R_i(x)$  to the constant 1 achieves the best trade-off curve between clean and attacked accuracy. Moreover, smoothing using the post-SoftMax probabilities outperforms the pre-SoftMax logits. This result aligns with the conclusions of Figure 1 and our theoretical analyses, demonstrating that various robust networks share the property of being more confident when classifying correctly than when making mistakes.

## B. Implementation of the mixing network in experiments

Since our formulation does not depend on the architecture of the base classifiers, Figure 3 presents the design of the mixing network in the context of general standard and robust classifiers. In the

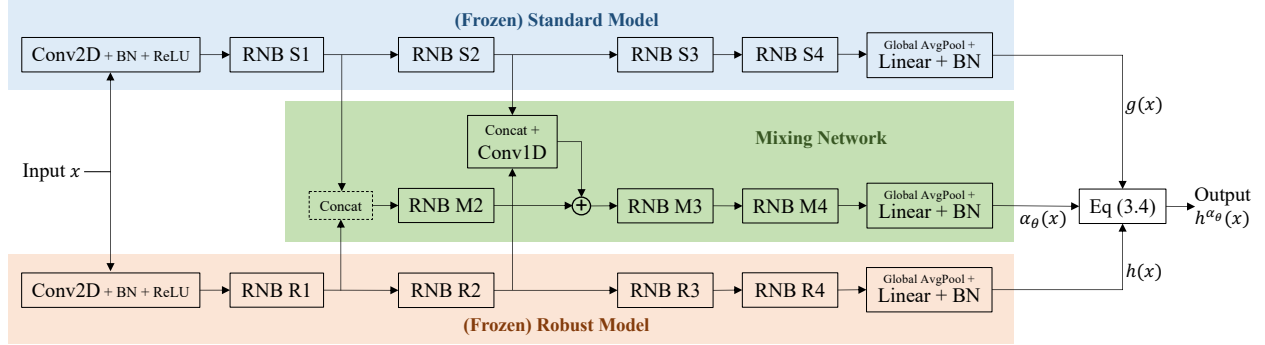


**Figure 7.** The architecture of the mixed classifier introduced in Section 4 when applied to a pair of ResNet base models.

experiments presented in Sec. 5.3, Both  $g(\cdot)$  and  $h(\cdot)$  are based on variants of the ResNet family, which share the general structure of having four main blocks. Thus, we present the structure of the mixed classifier with ResNet-like base models in Figure 7. Following [56], we consider the initial Conv2D layer and the first ResNet block as the upstream layers. The embeddings extracted by the first Conv2D layers in  $g(\cdot)$  and  $h(\cdot)$  are concatenated before being provided to the mixing network  $\alpha_\theta(\cdot)$ . We further select the second ResNet block as the middle layers. For this layer, in addition to concatenating the embeddings from  $g(\cdot)$  and  $h(\cdot)$ , we also attach a linear transformation layer (Conv1x1) to match the dimensions, reduce the number of features, and improve efficiency.

As mentioned in Sec. 4.1, the range of  $\alpha_\theta(\cdot)$  can be constrained to be within  $(\alpha_{\min}, \alpha_{\max}) \subseteq [0, 1]$  if certified robustness is desired. We empirically observe that setting  $\alpha_{\max} - \alpha_{\min}$  to be 0.1 or 0.15 works well. This observation coincides with Fig. 4, which shows that a slight increase in  $\alpha$  can greatly enhance the robustness at the most sensitive region. The value of  $\alpha_{\min}$  can then be determined by enforcing a desired level of either clean validation accuracy or robustness. Following this guideline, for the two models demonstrated in Table 4, we set the ranges of  $\alpha_\theta(\cdot)$  to be  $(0.84, 0.99)$  and  $(0.815, 0.915)$ , respectively. Note that this range is only applied during validation. When training  $\alpha_\theta(\cdot)$ , we use the full  $(0, 1)$  range for its output, so that the training-time adversary can generate strong and diverse attacks that fully exploit  $\alpha_\theta(\cdot)$ , which is crucial for securing the robustness of the mixing network.

## C. Ablation study in loss function hyperparameters

In this section, we discuss the effects of the constants  $c_{\text{CE}}$ ,  $c_{\text{BCE}}$ , and  $c_{\text{prod}}$  in the composite loss function (9). Since multiplying the three weight constants by the same number is equivalent to using a larger optimizer step size and is not the purpose of this ablation study, we fix  $c_{\text{CE}} + c_{\text{BCE}} = 1.5$ . To avoid the issue of becoming excessively conservative and always prioritizing the robust base model (as described in Section 4.4), we add a batch normalization layer without trainable affine transform to the output of the mixing network. Additionally, note that since the mixing network has a single output, one can arbitrarily shift this output to achieve the desired balance between clean and attacked accuracies. For a fair and illustrative comparison, after training a mixing network  $\alpha_\theta(\cdot)$  with each hyperparameter setting, we add an appropriate constant to the output of the  $\alpha_\theta(\cdot)$  so that the clean accuracy of the overall model  $h^{\alpha_\theta}(\cdot)$  is  $90 \pm 0.02\%$ , and compare the PGD<sub>20</sub> attacked

**Table 6.** The PGD<sub>20</sub> accuracy on CIFAR-10 with various loss hyperparameter settings. The setting is the same as in Table 2, and we consider both attack and defense in Setting B.

	$c_{\text{CE}} = 0$ $c_{\text{BCE}} = 1.5$	$c_{\text{CE}} = 0.5$ $c_{\text{BCE}} = 1$	$c_{\text{CE}} = 1$ $c_{\text{BCE}} = 0.5$	$c_{\text{CE}} = 1.5$ $c_{\text{BCE}} = 0$
$c_{\text{prod}} = 0$	54.5 %	52.8 %	53.8 %	54.4 %
$c_{\text{prod}} = 0.1$	54.3 %	54.1 %	54.0 %	54.1 %
$c_{\text{prod}} = 0.2$	55.1 %	54.2 %	54.3 %	53.9 %

**Table 7.** Compare various selections of the mixing network’s Sigmoid activation scaling factor.

Scale = 0.5	Scale = 1	Scale = 2	Scale = 4
55.1 %	55.5 %	55.7 %	55.6 %

accuracy of  $h^{\alpha\theta}(\cdot)$  in Table 6. As a baseline, when the smoothing strength  $\alpha$  is a constant, the PGD<sub>20</sub> accuracy is 52.6% when the clean accuracy is tuned to be 90% (the corresponding  $\alpha$  value is 1.763). The above results demonstrate that  $c_{\text{CE}} = 0$ ,  $c_{\text{BCE}} = 1.5$ , and  $c_{\text{prod}} = 0.2$  works the best.

Our results also show that a small positive  $c_{\text{prod}}$  is generally beneficial. This makes sense because the CE loss is low for a particular input if both  $g(\cdot)$  and  $h(\cdot)$  correctly predict its class. Thus, the smoothing strength should not matter for such input, and therefore the BCE loss is weighted by a small number. Compared with using only the BCE loss, the product term of the CE and the BCE components is lenient on inputs correctly classified by the mixed model  $h^{\alpha\theta}(\cdot)$ , while assigning more weight to the data that are incorrectly predicted.

Recall that the output range of  $\alpha_{\theta}(\cdot)$  is  $[0, 1]$ , which is enforced by appending a Sigmoid output activation function. In addition to shifting, one can arbitrarily scale the Sigmoid activation’s input. By performing this scaling, we effectively calibrate the confidence of the mixing network. In Table 6, this scaling is set to the same constant for all settings. In Table 7, we select the best loss parameter and analyze the validation-time Sigmoid scaling. Again, we shift the Sigmoid input so that the clean accuracy is  $90 \pm 0.02\%$ . While a larger scale benefits the performance on clean/attacked examples that are confidently recognized by the mixing network, an excessively large scale makes  $h^{\alpha\theta}(\cdot)$  less stable under attack. Table 7 shows that applying a scaling factor of 2 yields the best result for the given experiment setting.